Iterative Methods for Reconstructing PET Images

Peter A. Toft
Electronics Institute, Building 349
Technical University of Denmark
2800 Lyngby, Denmark
Phone +45 45934207
E-mail: ptoft@ei.dtu.dk

Version 1, 27/12-94

Abstract

In this report the fundamental theory of brain scanners is presented. It turns out that the wanted image of, e.g., the brain can be obtained by use of inverse Radon transformation. The Radon transform and several classical direct inversion schemes are presented. The inversion schemes are modified to enable a numerical implementation, and some of the numerical problems are discussed. The theory is extended into 3D and some theoretical aspects are presented. Finally some basic properties of the Radon transform are shown and a model of a brain named the Shepp Logan phantom is presented, which can be used to test numerical implementations of the inversion algorithms.

Contents

Abstract

In this report the fundamental theory of brain scanners is presented. It turns out that the wanted image of, e.g., the brain can be obtained by use of inverse Radon transformation. The Radon transform and several classical direct inversion schemes are presented. The inversion schemes are modified to enable a numerical implementation, and some of the numerical problems are discussed. The theory is extended into 3D and some theoretical aspects are presented. Finally some basic properties of the Radon transform are shown and a model of a brain named the Shepp Logan phantom is presented, which can be used to test numerical implementations of the inversion algorithms.

Chapter 1

Introduction

One of the most remarkable inventions in this century is the brain scanner. Over the years several types of scanners have emerged such as the CT-scanner (Computer Tomography), which is used for detection of the gamma ray absorption within the brain. Later the PET-scanner (Positron Emission Tomography) was developed, which makes it possible to monitor the activity of the brain. Other scanners are also available, but only CT- and PET-scanning are discussed in the following chapters.

Chapter 2

Fundamental Theory of the CT-Scanner

A CT-scanner is normally a ring with one X-ray emitter and a large number of detectors positioned opposite to the emitter, e.g., 750 detectors could be used. This is shown on Figure 2.1. Rotating the emitter and the detector array around the patient makes it possible to cover all parts of the brain. Note that the brain could be substituted by any structure with an interesting non-homogeneous interior hidden behind the surface.

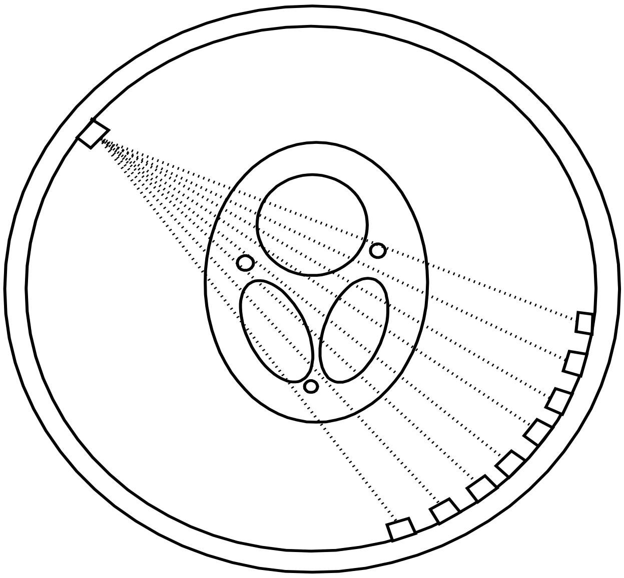

Figure 2.1: The CT Scanner

It can be assumed that the X-rays travel in straight lines, and the beam is attenuated along that line with the attenuation coefficient μ. After the scan the attenuation coefficient is to be found. It will be shown that this can be based on inversion of the Radon transform. If a planar CT-scanner with only one slice of the brain is measured, then the coordinate system can be chosen so that the slice is the $z = 0$ plane. Each line going through the scanned object is parameterized with two coordinates: The normal distance from $(0, 0)$ to the line ρ and the angle θ. These parameters are seen from Figure 2.2, where a phantom brain is shown.

If the scanned object is non-homogeneous then the attenuation coefficient is a function of x and y, i.e., $\mu(x, y)$. Assume that the emitter and one of the detectors define the line (ρ, θ). On Figure 2.3 three

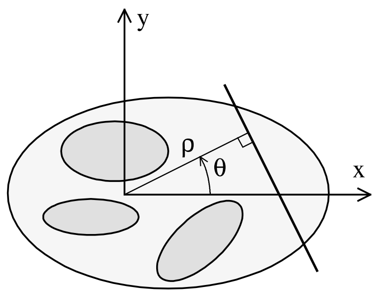

Figure 2.2: Parameters used to describe the lines

different objects are shown (seen along the line).

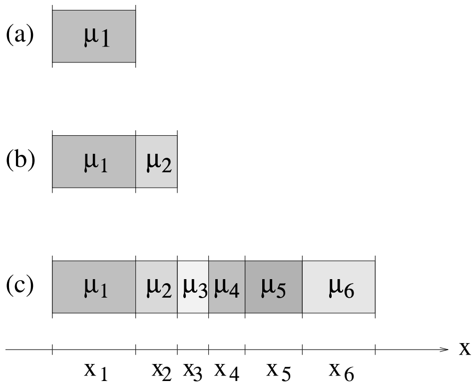

Figure 2.3: Three different media, with attenuation coefficients μ and a widths x.

In case (a) the received intensity is given by

$$I(\rho,\theta) = I_0\ e^{-\mu_1 x_1} \tag{2.1}$$

If two different homogeneous media are penetrated as shown at (b) the received intensity is

$$I(\rho,\theta) = I_0\ e^{-\mu_1 x_1 - \mu_2 x_2} \tag{2.2}$$

If several homogeneous media are present, like in case (c), then the result is that

$$I(\rho,\theta) = I_0\ e^{-\sum_i \mu_i x_i} \tag{2.3}$$

In the general form, where the attenuation coefficient is a function of the line path, then the sum in Equation 2.3 will become an integral and x_i becomes the line element ds.

$$I(\rho,\theta) = I_0\ e^{-\int \mu(x,y)\ ds} \tag{2.4}$$

In this Equation the parameter I_0 is the intensity of the emitter, and s denotes the parameter in the normal form of the line, where (x, y) lies on the line defined by (ρ, θ). From Equation 2.4 the projection $\mathcal{P}(\rho, \theta)$ is defined

$$\mathcal{P}(\rho,\theta) = \log\left(\frac{I_0}{I(\rho,\theta)}\right) = \int \mu(x,y)\ ds = \int_{-\infty}^{\infty} \mu(\rho\cos\theta - s\sin\theta, \rho\sin\theta + s\cos\theta)\ ds \tag{2.5}$$

Using the Dirac delta function the projections can be rewritten

$$\begin{aligned}
\mathcal{P}(\rho,\theta) &= \frac{1}{|\sin\theta|}\int_{-\infty}^{\infty}\mu\left(x, \frac{\rho}{\sin\theta} - x\cot\theta\right)\,dx & (2.6)\\
&= \frac{1}{|\sin\theta|}\int_{-\infty}^{\infty}\int_{-\infty}^{\infty}\mu(x,y)\;\delta\left(y - \frac{\rho}{\sin\theta} + x\cot\theta\right)\,dx\;dy & (2.7)\\
&= \int_{-\infty}^{\infty}\int_{-\infty}^{\infty}\mu(x,y)\;\delta(\rho - x\cos\theta - y\sin\theta)\;dx\;dy & (2.8)
\end{aligned}$$

In the mathematical literature [5, 13, 23] it can be recognized that $\mathcal{P}(\rho,\theta)$ is the Radon transform of $\mu(x,y)$. Using the mathematical symbols the Radon transform of a function $g(x,y)$ is defined by

$$\check{g}(\rho,\theta) = \int_{-\infty}^{\infty}\int_{-\infty}^{\infty} g(x,y)\;\delta(\rho - x\cos\theta - y\sin\theta)\;dx\;dy \qquad (2.9)$$

This means that the attenuation coefficient $\mu(x,y)$ can be found from the projections using the inverse Radon transform.

In the literature [5, 15, 13] direct inversion schemes can be found. One class is based on the *Central Slice Theorem*, which is implemented using 1D Fast Fourier Transformation, 2D Fast Fourier transformation and 2D interpolation. This will normally result in a very fast algorithm, but numerical artifacts due to the interpolation can decrease the performance. Another 'famous' inversion scheme is the *Filtered Backprojection* which is a combination of filtering and integration. This inversion scheme is commonly used in medical scanners due to good numerical stability, but the algorithm will normally be somewhat slow.

In conclusion, it can be noted that the CT-scan gives a map of the attenuation coefficient. The CT-scanners have been used several years. The current trend is to perform helical CT, where the emitter and detector ring rotate around the patient and make a uniform motion along the z-axis, as shown on Figure 2.4.

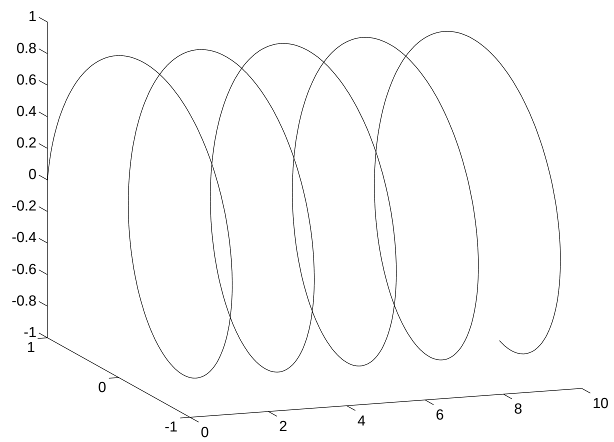

Figure 2.4: Motion of the emitter when using helical CT scanning

In this way a 3D-image of the interior can be obtained with a better resolution compared to a large number of plane scans placed along the z-axis. From the attenuation coefficient CT-scanners reveal little information of the brain activity. To gain this information PET-scanners have been developed.

Chapter 3

The PET Scanner

The PET scanner is based on another type of measurement. A small dosage of a β^+ emitter, such as O-15 or C-11, is injected into the patient (or the object to be scanned). The β^+ emitter will be circulated in the tissue due to the blood circulation. If for instance the brain is to be scanned then the β^+ emitter will decay in correspondence to the activity of the brain. In the regions with high brain activity the blood flow will be high, and many of the radioactive nucleons will decay under emission of a positron in these regions. Within a few mm the positron will interact with an electron and annihilate under emission of two 511 keV photons. The two photons will travel in opposite directions outward to the PET scanner where the photons are detected at sensors placed in a ring, as illustrated on Figure 3.1. Note that only detectors are needed, as the emitter is placed within the patient.

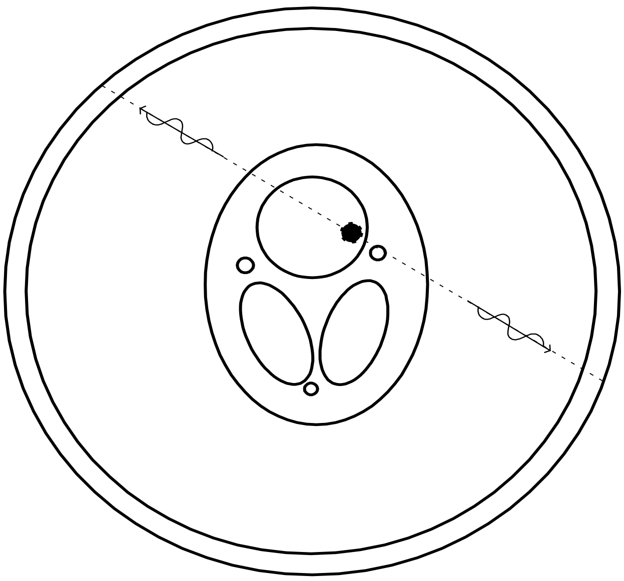

Figure 3.1: Emission of two photons from the place of decay.

On Figure 3.2 is shown a real PET scanner - the General Electric Advance, photographed at the National University Hospital in Copenhagen.

On Figure 3.3 is shown the same scanner with the front opened. Note the detectors are visible.

The PET hardware will sort the arrival times of the photons, so only two photons that arrived at

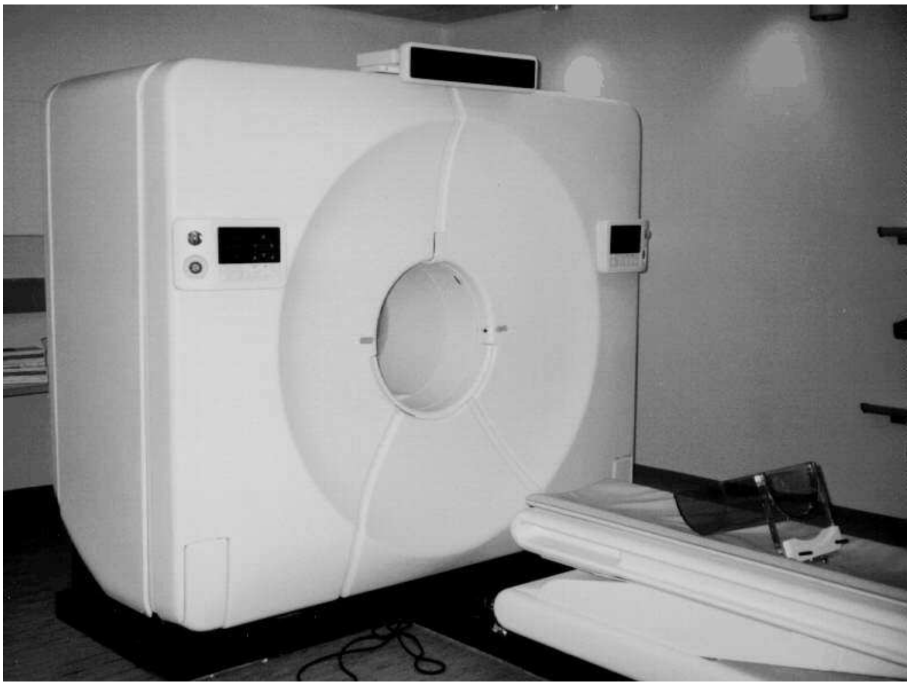

Figure 3.2: The GE Advance PET scanner.

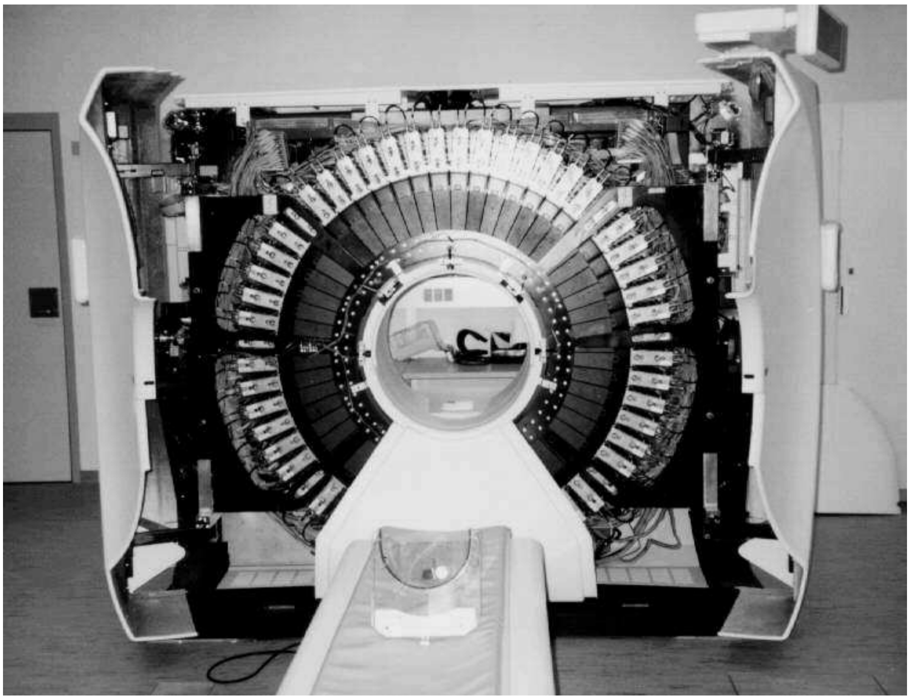

Figure 3.3: The GE Advance PET scanner opened.

the same time at the sensor ring are taken into account[1]. A two dimensional matrix of the possible line parameters is created, i.e., $E(\rho,\theta)$. If the two photons form a line with parameters $(\rho,\theta) = (\rho_0,\theta_0)$, then the array is incremented with the value one at that position in the array. This is because the only obtainable information from the two photons is that the photon emission took place somewhere along that line. Depending on the radioactive dose given to the patient many decays take place per second in each volume element. After the recording is terminated an array of emissions has been recorded. For $(\rho,\theta) = (\rho_0,\theta_0)$ the array (now assumed to be continuous in both parameters) is developed by several β^+ emissions which took place along the line. The individual emission recordings are no longer stored. The obtained array of emissions (called the *sinogram*) are in each position approximately proportional to the emission intensity along that particular line (times the total recording time T). The obtained matrix divided by T is in mathematical terms an integral of the emission intensity $A(x,y)$ over that particular line. If the measured matrix is named $E(\rho,\theta)$ then

$$E(\rho,\theta) = \int_{-\infty}^{\infty}\int_{-\infty}^{\infty} A(x,y)\ \delta(\rho - x\cos\theta - y\sin\theta)\ dx\ dy\ T \tag{3.1}$$

Again it can be recognized that the recorded array $E(\rho,\theta)$ is the Radon transform of the emission intensity $A(x,y)$. Note that this intensity will not be a constant in time as it varies with the activity of the brain. This may limit the allowable recording time. Previously absorption of the photons in the tissue has been neglected, thus the inversion process must be modified to take this into account. This is rather easy when using double photon emissions. The activity of the brain can be split up in a sum of point sources. Now the point source in a fixed place $(x,y) = (x_0,y_0)$ is considered. Assume that in the time window τ_e, $A(x_0,y_0)$ pairs of photons are produced, which lie on the line $(\rho,\theta) = (\rho_0,\theta_0)$. Assume that the attenuation cannot be neglected and that projections $\mathcal{P}(\rho,\theta)$ have been measured using the transmission tomography as discussed in chapter 2. Now consider two photons traveling from (x_0,y_0), as shown on Figure 3.4.

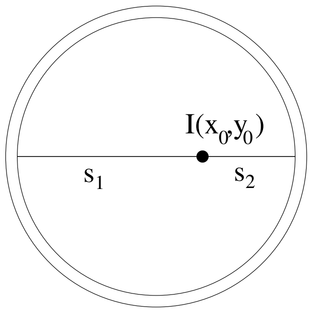

Figure 3.4: Emission of two photons from (x_0,y_0) along the line (ρ,θ).

The photon traveling along the line piece s_1 will reach the detector ring with the probability P_1.

$$P_1 = e^{-\int_{s1}\mu(x,y)\ ds} \tag{3.2}$$

This is the result from chapter 2, see Equation 2.4. The other photon traveling in the opposite direction along s_2 will reach the opposite detector with the probability P_2.

$$P_2 = e^{-\int_{s2}\mu(x,y)\ ds} \tag{3.3}$$

The two photons travel independently, which imply that the probability of detecting both photons is the

[1]The photons travel with the speed of light, and here is the small difference in arrival time neglected

product of P_1 and P_2. This means that the measured matrix of emissions $E(\rho,\theta)$ from the point source is given by

$$\begin{aligned}
E(\rho,\theta) &= A(x_0,y_0)\ P_1\ P_2 && (3.4)\\
&= A(x_0,y_0)\ e^{-\int_{s1}\mu(x,y)\ ds}\ e^{-\int_{s2}\mu(x,y)}\ ds && (3.5)\\
&= A(x_0,y_0)\ e^{-\int_{s}\mu(x,y)\ ds} && (3.6)
\end{aligned}$$

where the integral in the last line is the integral of the attenuation coefficient along the line (ρ,θ), which contains (x_0,y_0). If all point sources in the brain are considered then the measured matrix is

$$\begin{aligned}
E(\rho,\theta) &= \int A(x_0,y_0)e^{-\int_s \mu(x,y)\ ds}\ ds_0\ \tau_e && (3.7)\\
&= e^{-\int_s \mu(x,y)\ ds}\int_s A(x,y)\ d\ \tau_e s && (3.8)\\
&= e^{-P(\rho,\theta)}\int_s A(x,y)\ ds\ \tau_e\ \Rightarrow && (3.9)\\
\breve{A}(\rho,\theta) &= \int_s A(x,y)\ ds && (3.10)\\
&= \int_{-\infty}^{\infty}\int_{-\infty}^{\infty} A(x,y)\ \delta(\rho - x\cos\theta - y\sin\theta)\ dx\ dy && (3.11)\\
&= \frac{E(\rho,\theta)}{\tau_e}\ e^{\mathcal{P}(\rho,\theta)} && (3.12)
\end{aligned}$$

where s_0 denotes integration with respect to (x_0,y_0) along the line (ρ_0,θ_0). Note that the attenuation factor becomes a constant (along that line). Note also that the transmission scan is used in the Radon domain, no inversion of $P(\rho,\theta)$ is needed. The result is that the attenuation coefficient only produces a multiplicative factor in the Radon domain. This imply that the essential part of producing brain images still is based on inversion of the Radon transform, which is the subject of the next chapter.

3.1 The Two Transmission Scans

In order to obtain a estimate of $\mathcal{P}(\rho,\theta)$ the normalization factor I_0 is needed. Up to this point this factor has been assumed to be a constant. This is not true, but this error is easily corrected using another transmission scan, the *Blank Scan*, prior to the two other scans. Without the patient a transmission scan is done by measuring the transmitted photon intensity or rather the total number of photons transmitted along the line (ρ,θ) for τ_b seconds, this gives $B(\rho,\theta)$. After the patient is placed in the scanner another transmission scan is recorded for τ_t seconds. This gives the transmission matrix $T(\rho,\theta)$. Assume that in both scans $I_0(\rho,\theta,x_r,y_r)$ is transmitted per second from the radioactive source along the line with parameters (ρ,θ) to the detecter at position (x_r,y_r). Neglecting the absorption in air the measured matrix B is given by

$$B(\rho,\theta) = \tau_b\ I_0(\rho,\theta,x_r,y_r)\ e^{-\int \mu_{\text{hardware}}\ ds} \qquad (3.13)$$

where the label 'hardware' indicates that some parts of the scanner cannot be avoided when measuring the blank scan along tha particular line. This could be a plastic cover and a bed for the patient.

With the patient in the scanner the transmission matrix T is slightly different due to the absorption in the patient.

$$T(\rho,\theta) = \tau_t\ I_0(\rho,\theta,x_r,y_r)\ e^{-\int \mu_{\text{hardware}}\ ds}\ e^{-\int \mu_{\text{patient}}\ ds} \qquad (3.14)$$

From Equation 3.13 and 3.14 the attenuation factor is easily found

$$e^{\int \mu_{\text{patient}}\ ds} = \frac{B(\rho,\theta)\ \tau_t}{T(\rho,\theta)\ \tau_b} \tag{3.15}$$

This implies that the Radon transform of the activity corrected for attenuation (cf. Equation 3.12) is given by

$$\breve{A}(\rho,\theta) = \frac{E(\rho,\theta)\ B(\rho,\theta)\ \tau_t}{T(\rho,\theta)\ \tau_e\ \tau_b} \tag{3.16}$$

This equation reveals some potential problems. The corrected sinogram $\breve{A}$ is highly dependent on any low value in the transmission scan as it appears in the denominator. This issue is further discussed in chapter 9.

From this sinogram is the activity derived by using the inverse Radon transform. This is the subject of the next chapter.

Chapter 4

Inversion of the Radon Transform

In this chapter several invertion schemes are presented. It can be noted that other inversion schemes are available.

4.1 The Fourier Slice Theorem

Inversion of the Radon transform can be achieved in several ways. One standard algorithm is based on the *Fourier Slice Theorem* also known as *Central Slice Theorem* [16]. The Radon transform $\check{g}(\rho,\theta)$ is to be inverted into $g(x,y)$. The inversion is based on the Fourier transform (FT). First the 2D-FT of $g(x,y)$ is calculated.

$$G(\sigma,\gamma)=\int_{-\infty}^{\infty}\int_{-\infty}^{\infty} g(x,y)\ e^{-j2\pi(\sigma x+\gamma y)}\ dx\ dy \tag{4.1}$$

And the inverse transform is given by

$$g(x,y)=\int_{-\infty}^{\infty}\int_{-\infty}^{\infty} G(\sigma,\gamma)\ e^{j2\pi(\sigma x+\gamma y)}\ d\sigma\ d\gamma \tag{4.2}$$

Now polar frequency parameters are introduced

$$\begin{pmatrix}\sigma\\ \gamma\end{pmatrix}=\nu\ \begin{pmatrix}\cos\theta\\ \sin\theta\end{pmatrix} \tag{4.3}$$

Inserting the polar frequencies in equation 4.1 gives

$$\begin{aligned} G(\nu\ \cos\theta,\nu\ \sin\theta) &= \int_{-\infty}^{\infty}\left[\int_{-\infty}^{\infty}\int_{-\infty}^{\infty} g(x,y)\ \delta(\rho-x\cos\theta-y\sin\theta)\ e^{-j2\pi\rho\nu}\ dx\ dy\right]\ d\rho \\ &= \int_{-\infty}^{\infty}\left[\int_{-\infty}^{\infty}\int_{-\infty}^{\infty} g(x,y)\ \delta(\rho-x\cos\theta-y\sin\theta)\ dx\ dy\right]\ e^{-j2\pi\rho\nu}\ d\rho \\ &= \int_{-\infty}^{\infty}\check{g}(\rho,\theta)\ e^{-j2\pi\rho\nu}\ d\rho \end{aligned} \tag{4.4}$$

Thus a one-dimensional FT of the Radon transform gives the spectrum, which subsequently gives $g(x,y)$, cf. Equation 4.2. The Fourier Slice Theorem can be summerized as

$$G(\nu\ \cos\theta,\nu\ \sin\theta) = \int_{-\infty}^{\infty}\check{g}(\rho,\theta)\ e^{-j2\pi\rho\nu}\ d\rho \tag{4.5}$$

$$g(x,y) = \int_{-\infty}^{\infty}\int_{-\infty}^{\infty} G(\sigma,\gamma)\ e^{j2\pi(\sigma x+\gamma y)}\ d\sigma\ d\gamma \tag{4.6}$$

The Fourier Slice Theorem makes it possible to invert the Radon transform by use of 1D Fourier transforms and 2D Fourier transforms. Note that the theorem can be used in reverse to calculate the Radon transform, if the signal $g(x, y)$ is given.

4.2 Filtered Backprojection

Another common inversion scheme is the *Filtered Backprojection* method [25, 24]. It is derived from equation 4.2, where the polar coordinates are used

$$\begin{aligned} g(x,y) &= \int_0^{2\pi}\int_0^{\infty} \nu\, G(\nu\cos\theta, \nu\cos\theta)\; e^{j2\pi\nu(x\cos\theta + y\sin\theta)}\; d\nu\; d\theta \\ &= \int_0^{\pi}\int_{-\infty}^{\infty} |\nu|\; G(\nu\cos\theta, \nu\cos\theta)\; e^{j2\pi\nu(x\cos\theta + y\sin\theta)}\; d\nu\; d\theta \\ &= \int_0^{\pi}\int_{-\infty}^{\infty} |\nu| \left[\int_{-\infty}^{\infty} \breve{g}(\tilde{\rho},\theta)\; e^{-j2\pi\tilde{\rho}\nu}\; d\tilde{\rho}\right] e^{j2\pi\nu(x\cos\theta + y\sin\theta)}\; d\nu\; d\theta \qquad (4.7) \end{aligned}$$

Equation 4.7 can be written in two parts: A filtering part and an integration part.

$$\begin{aligned} g^{\dagger}(\rho,\theta) &= \int_{-\infty}^{\infty} |\nu| \left[\int_{-\infty}^{\infty} \breve{g}(\tilde{\rho},\theta)\; e^{-j2\pi\tilde{\rho}\nu}\; d\tilde{\rho}\right] e^{j2\pi\rho\nu}\; d\nu \qquad (4.8) \\ &= \mathrm{IFT}_{\nu\to\rho}\left\{|\nu|\; \mathrm{FT}_{\tilde{\rho}\to\nu}\left\{\breve{g}(\tilde{\rho},\theta)\right\}\right\} \qquad (4.9) \end{aligned}$$

$$\begin{aligned} g(x,y) &= \int_0^{\pi} g^{\dagger}(x\cos\theta + y\sin\theta, \theta)\; d\theta \qquad (4.10) \\ &= \int_0^{\pi}\int_{-\infty}^{\infty} g^{\dagger}(\rho,\theta)\; \delta(\rho - x\cos\theta - y\sin\theta)\; d\rho\; d\theta \qquad (4.11) \end{aligned}$$

Equation 4.10 is named the adjoint Radon transform or the backprojection due to the similarity to the forward Radon transform, cf. equation 2.9. The filtering part in equation 4.8 is a forward Fourier transform for each of the angles. In the Fourier domain the signal is high pass filtered with the filter $|\nu|$. Finally an inverse 1D-Fourier transform is used to get the filtered Radon domain $g^{\dagger}(\rho, \theta)$. The adjoint Radon transform is merely an integration along a sine-curve in the filtered Radon domain. Equation 4.8 and 4.10 is the filtered backprojection inversion scheme.

Filtered Backprojection can also be expressed without using filtering in the frequency domain. The filter $|\nu|$ is expressed as a product.

$$\begin{aligned} |\nu| &= \frac{-j\ \mathrm{sign}(\nu)}{2\pi}\; j2\pi\nu\ \Rightarrow \qquad (4.12) \\ g^{\dagger}(\rho,\theta) &= \mathrm{IFT}_{\nu\to\rho}\left\{\frac{-j\ \mathrm{sign}(\nu)}{2\pi}\; j2\pi\nu\; \mathrm{FT}_{\tilde{\rho}\to\nu}\left\{\breve{g}(\tilde{\rho},\theta)\right\}\right\} \qquad (4.13) \\ &= \frac{1}{2\pi^2\rho} * \frac{\partial\breve{g}(\rho,\theta)}{\partial\rho} \qquad (4.14) \end{aligned}$$

Here the Hilbert transform of a function is introduced.

$$\begin{aligned} \mathcal{H}g(t) &= \frac{1}{\pi}\int_{-\infty}^{\infty} \frac{g(t')}{t - t'}\; dt' \Rightarrow \qquad (4.15) \\ g^{\dagger}(\rho,\theta) &= \frac{1}{2\pi}\mathcal{H}\frac{\partial\breve{g}(\rho,\theta)}{\partial\rho} \qquad (4.16) \end{aligned}$$

In total filtered backprojection can be summarized as.

$$g(x,y) = \frac{1}{2\pi}\int_0^{\pi} (\mathcal{H}\frac{\partial \breve{g}(\rho,\theta)}{\partial \rho})_{\rho = x\cos\theta + y\sin\theta}\ d\theta \tag{4.17}$$

Discrete implementation from Equation 4.17 is rather problematic, because of the Hilbert transformation. The Hilbert transform cannot be implemented easily without using Fourier transformation. If this is the case then the reconstruction formula matches the one given in Equation 4.8 and 4.10.

4.3 Filtering after Backprojection

It is also possible to make the backprojection, i.e. the adjoint Radon transform before the filtering. In this case another filter must be used. Rewriting $g(x,y)$ using the delta function gives

$$\begin{aligned} g(x,y) &= \int_{-\infty}^{\infty}\int_{-\infty}^{\infty} g(x_0,y_0)\ \delta(x-x_0)\ \delta(y-y_0)\ dx_0\ dy_0\ \Rightarrow && (4.18)\\ \breve{g}(\rho,\theta) &= \int_{-\infty}^{\infty}\int_{-\infty}^{\infty} g(x_0,y_0)\ \delta(\rho - x_0\cos\theta - y_0\sin\theta)\ dx_0\ dy_0 && (4.19) \end{aligned}$$

Equation 4.19 shows that each point (x_0, y_0) is transformed into a sine curve in the Radon domain. The Radon transform of $g(x,y)$ is the sum (integral) of all the sine curves in the Radon domain. In the following the integrations over x_0 and y_0 are omitted. This can be done because only linear transforms are used. Now assume a point source is given and the adjoint Radon transform is applied before a filtering.

$$\begin{aligned} g(x,y) &= \delta(x-x_0)\ \delta(y-y_0)\ \Rightarrow && (4.20)\\ \breve{g}(\rho,\theta) &= \delta(\rho - x_0\cos\theta - y_0\sin\theta) && (4.21)\\ \tilde{g}(x,y) &= \int_0^{\pi} \breve{g}(x\cos\theta + y\sin\theta, \theta)\ d\theta && (4.22)\\ &= \left.\frac{1}{|(x-x_0)\sin\theta - (y-y_0)\cos\theta|}\right|_{(x-x_0)\cos\theta + (y-y_0)\sin\theta = 0} && (4.23)\\ &= \frac{1}{\left|-(x-x_0)\sin\arctan\left(\frac{x-x_0}{y-y_0}\right) - (y-y_0)\cos\arctan\left(\frac{x-x_0}{y-y_0}\right)\right|} && (4.24)\\ &= \frac{\sqrt{1+\left(\frac{x-x_0}{y-y_0}\right)^2}}{\frac{(x-x_0)^2}{y-y_0} + (y-y_0)} = \frac{1}{\sqrt{(x-x_0)^2 + (y-y_0)^2}} && (4.25) \end{aligned}$$

It can be recognized that this is a two dimensional convolution.

$$\begin{aligned} \tilde{g}(x,y) &= g(x,y) * h(x,y) && (4.26)\\ h(x,y) &= \frac{1}{\sqrt{x^2+y^2}} && (4.27) \end{aligned}$$

Using the technique shown in Equation 4.19 it can be seen that Equation 4.26 is valid for any given $g(x,y)$, Equation 4.26 thus enables another inversion scheme. A two dimensional Fourier transform of Equation 4.26 gives

$$\begin{aligned} \tilde{G}(\sigma,\gamma) &= G(\sigma,\gamma)\ H(\sigma,\gamma) \Rightarrow && (4.28)\\ G(\sigma,\gamma) &= \frac{\tilde{G}(\sigma,\gamma)}{H(\sigma,\gamma)} && (4.29) \end{aligned}$$

From standard 2D Fourier transform tables it can be found that

$$h(x,y) = \frac{1}{\sqrt{x^2+y^2}} \;\leftrightarrow\; H(\sigma,\gamma) = \frac{1}{\sqrt{\sigma^2+\gamma^2}} \tag{4.30}$$

This means that $g(x,y)$ can be found as

$$\tilde{g}(x,y) = \int_0^{\pi} \check{g}(x\cos\theta + y\sin\theta, \theta)\; d\theta \tag{4.31}$$

$$\tilde{G}(\sigma,\gamma) = \int_{-\infty}^{\infty}\int_{-\infty}^{\infty} \tilde{g}(x,y)\; e^{-j2\pi(\sigma x+\gamma y)\; dx\; dy} \tag{4.32}$$

$$g(x,y) = \int_{-\infty}^{\infty}\int_{-\infty}^{\infty} \sqrt{\sigma^2+\gamma^2}\; \tilde{G}(\sigma,\gamma)\; e^{j2\pi(\sigma x+\gamma y)}\; d\sigma\; d\gamma \tag{4.33}$$

Filtering after backprojection makes use of an integration succeeded by a two dimensional high pass filtering. This is an inversion algorithm very similar to filtered backprojection.

Chapter 5

Calculation using Operators

A number of textbooks, e.g. [5, 6], define operators. In this section relevant operators are defined, which will enable an easy way to write the inversion algorithms. In the following x, y, σ and γ denotes continuous variables. To identify the continuous operators calligrafic letters are used, e.g., $\mathcal{R}$.

$$\mathcal{R}g(x,y) = \breve{g}(\rho,\theta) = \int_{-\infty}^{\infty}\int_{-\infty}^{\infty} g(x,y)\ \delta(\rho - x\cos\theta - y\sin\theta)\ dx\ dy \tag{5.1}$$

$$\mathcal{B}h(\rho,\theta) = \int_0^{\pi} h(x\cos\theta + y\sin\theta, \theta)\ d\theta \tag{5.2}$$

$$\mathcal{F}_{p1}^{-}h(\rho,\theta) = \int_{-\infty}^{\infty} h(\tilde{\rho},\theta)\ e^{-j2\pi\tilde{\rho}\nu}\ d\tilde{\rho} \tag{5.3}$$

$$\mathcal{F}_{p1}^{+}H(\nu,\theta) = \int_{-\infty}^{\infty} H(\nu,\theta)\ e^{j2\pi\rho\nu}\ d\nu \tag{5.4}$$

$$\mathcal{F}_{r2}^{-}h(x,y) = \int_{-\infty}^{\infty}\int_{-\infty}^{\infty} h(\tilde{x},\tilde{y})\ e^{-j2\pi(\sigma\tilde{x}+\gamma\tilde{y})}d\tilde{x}\ d\tilde{y} \tag{5.5}$$

$$\mathcal{F}_{r2}^{+}H(\sigma,\gamma) = \int_{-\infty}^{\infty}\int_{-\infty}^{\infty} H(\sigma,\gamma)\ e^{j2\pi(\sigma x+\gamma y)}d\sigma\ d\gamma \tag{5.6}$$

$$\mathcal{C}h(\rho,\theta) = \int_{-\infty}^{\infty} |\nu| \int_{-\infty}^{\infty} h(\tilde{\rho},\theta)\ e^{-j2\pi\tilde{\rho}\nu}d\tilde{\rho}\ e^{j2\pi\rho\nu}\ d\rho \tag{5.7}$$

$$\mathcal{D}h(x,y) = \int_{-\infty}^{\infty}\int_{-\infty}^{\infty} \sqrt{\sigma^2+\gamma^2} \int_{-\infty}^{\infty}\int_{-\infty}^{\infty} h(\tilde{x},\tilde{y})\ e^{-j2\pi(\sigma\tilde{x}+\gamma\tilde{y})}d\tilde{x}\ d\tilde{y}\ e^{j2\pi(\sigma x+\gamma y)}\ d\sigma\ d\gamma \tag{5.8}$$

Using the symbolic operators it is easy to express the presented inversion algorithms in a short form

$$\text{Filtered Backprojection}: \mathcal{B}\mathcal{F}_{1p}^{+}\ |\nu|\ \mathcal{F}_{1p}^{-}\ \breve{g} = \mathcal{B}\mathcal{C}\ \breve{g} = g(x,y) \Leftrightarrow \tag{5.9}$$

$$\mathcal{B}\mathcal{F}_{1p}^{+}\ |\nu|\ \mathcal{F}_{1p}^{-}\ \mathcal{R} = \mathcal{B}\mathcal{C}\mathcal{R} = \mathcal{I} \tag{5.10}$$

where $\mathcal{I}$ is the unity operator, i.e., $\mathcal{I}g = g$.

$$\text{Filtering after Backprojection}: \mathcal{F}_{2r}^{+}\ \sqrt{\sigma^2+\gamma^2}\ \mathcal{F}_{2r}^{-}\ \mathcal{B}\ \breve{g} = \mathcal{D}\mathcal{B}\breve{g} = g(x,y) \Leftrightarrow \tag{5.11}$$

$$\mathcal{F}_{2r}^{+}\ \sqrt{\sigma^2+\gamma^2}\ \mathcal{F}_{2r}^{-}\ \mathcal{B}\ \mathcal{R} = \mathcal{D}\mathcal{B}\mathcal{R} = \mathcal{I} \tag{5.12}$$

In the same way the Central Slice Theorem can be written

$$\text{Central Slice Theorem}: \mathcal{F}_{2r}^{+}\ \mathcal{F}_{1p}^{-}\ \breve{g} = g(x,y) \Leftrightarrow \tag{5.13}$$

$$\mathcal{F}_{2r}^{+}\ \mathcal{F}_{1p}^{-}\ \mathcal{R} = \mathcal{I} \tag{5.14}$$

where a conversion between polar and rectangular frequency coordinates is implied.

5.1 The Zero Frequency Problem

In the previous sections a perfect inversion is assumed, cf., e.g., Equation 5.12, but the two backprojections algorithms cannot invert perfectly,due to the filters used in the inversion. Using Filtered Backprojection it is seen that the polar spectrum at zero frequency ($\nu = 0$) is multiplied with zero. This will in practice imply that a possible DC-value cannot be obtained. Using Backprojection after Filtering it is obvious that the zero frequency value of the inverted signal $g(x, y)$ must be zero. The Central Slice Theorem does not have this built-in problem, but as it will be shown, the Central Slice Theorem is somewhat problematic to implement, and the two backprojection algorithms by far easier. The numerical stabilities of the presented inversion schemes are very different.

Chapter 6

Considerations before Implementation

Both the Central Slice Theorem and the Filtered Backprojection inversion schemes can be implemented using a sum approximation for the adjoint Radon transform and FFT/IFFT for the Fourier transforms. Though several problems and effects must be dealt with before implementation can be done. This will surely enhance the performance of the numerical algorithms.

6.1 Sampling

In most implementations a linear sampling of all variables is used.

$$\begin{array}{lllllll} x & = & x_m & = & x_{low} + m\Delta X & m = 0, 1, ..., M-1 \\ y & = & y_n & = & y_{low} + n\Delta Y & n = 0, 1, ..., N-1 \\ \rho & = & \rho_r & = & \rho_{low} + r\Delta\rho & r = 0, 1, ..., R-1 \\ \theta & = & \theta_t & = & \theta_{low} + t\Delta\theta & t = 0, 1, ..., T-1 \end{array} \tag{6.1}$$

Note that this choice will in general not give an optimum numerical stability, but aids a fairly easy implementation. See [15] for more information concerning non-linear sampling of the parameter domain.

It is easily verified that $\breve{g}(\rho, \theta) = \breve{g}(-\rho, \theta + \pi)$. This gives a choice when choosing datastructure. It is possible to choose $\rho \geq 0$, which normally imply that $0 \leq \theta < 2\pi$. It is also possible to choose $0 \leq \theta < \pi$ and ρ both positive and negative. This choice must be done considering the specific implementation. In the following it is chosen to use $0 \leq \theta < \pi$, which implies that $\Delta\theta = \frac{\pi}{T}$.

When implementing a Radon (or inverse Radon) transformation several things must be fulfilled, to insure a reasonable parameter choice. Firstly sampling must be adequate in all parameters. This will imply upper bounds on the sampling intervals. Secondly it must be assumed that the signal to be transformed $g(x, y)$ is zero if $\sqrt{x^2 + y^2} > |\rho_{max}|$. This demand will insure that $\breve{g}(\rho, \theta) = 0$ if $|\rho| > |\rho_{max}|$. If this cannot be fulfilled, numerical problems must be expected, because a numerical implementation must use a finite data array, which is not sufficient, if $g(x, y)$ is unlimited.

If $g(x, y)$ can be limited, then $(x, y) = (0, 0)$ should be placed to minimize $|\rho_{max}|$. This will reduce the size of the data array (with respect to ρ) used for the discrete Radon transform. Normally ρ_r is placed symmetrically around $\rho = 0$, and r is chosen to be odd. In this case

$$\rho_{min} = -\Delta\rho \, \frac{R-1}{2} \tag{6.2}$$

is used. This choice implies that $|\rho_{min}| = |\rho_{max}|$. The parameter R can then be chosen to fulfill $\sqrt{x^2 + y^2} < |\rho_{max}|$, where (x, y) is the point with longest distance to $(0, 0)$ in the scanned object.

Normally the object to be scanned does not change significantly when rotated. This implies that $\Delta X = \Delta Y$ is a rational choice.

The remaining parameters can be chosen according to the needed precision and the computational capacity. This is discussed in [26]. The result is that a reasonable choice is $\Delta\rho = \Delta X = \Delta Y$ and $\Delta\theta = \frac{\Delta X}{\sqrt{2}|\rho_{min}|}$. Normally $\Delta\rho$ is defined by the PET hardware. If this is not true it can be set to the wanted resolution.

6.2 Sampling in the Parameter Domain

Assume the Radon transform of a two dimensional signal given with a certain resolution. This could come from, e.g., a PET-scanner. Then some theoretical bounds on the resolution in the reconstructed image could be in place. Assume that the two dimensional function $g(x, y)$ is sampled according to the sampling criterion.

$$g_d(m,n) = g(x_{low} + m\Delta X, y_{low} + n\Delta Y) \tag{6.3}$$

From the discrete image $g_d(m, n)$ it is possible to find $g(x, y)$ by convoluting with a two dimensional sinc-function. Here it is assumed that the finite set of samples is sufficient to discribe the continuous function and that $\Delta X = \Delta Y$.

$$g(x,y) = \sum_{m=0}^{M-1}\sum_{n=0}^{N-1} g_d(m,n)\, \frac{\sin\left(\frac{\pi}{\Delta X}(x - m\Delta X - x_{low})\right)}{\left(\frac{\pi}{\Delta X}(x - m\Delta X - x_{low})\right)}\, \frac{\sin\left(\frac{\pi}{\Delta X}(y - n\Delta X - y_{low})\right)}{\left(\frac{\pi}{\Delta X}(y - n\Delta X - y_{low})\right)} \tag{6.4}$$

The basic idea in the following is to calculate the Radon transform of the function $g(x, y)$ given in Equation 6.4. The calculation is taken from [26].

$$\begin{aligned}
\breve{g}(\rho,\theta) &= \int_{-\infty}^{\infty} g(\rho\cos\theta - s\sin\theta, \rho\sin\theta - s\cos\theta)\, ds && (6.5)\\
&= \sum_{m=0}^{M-1}\sum_{n=0}^{N-1} g_d(m,n) \int_{-\infty}^{\infty} \frac{\sin\left(\frac{\pi}{\Delta X}(x - m\Delta X - x_{low})\right)}{\frac{\pi}{\Delta X}(x - m\Delta X - x_{low})}\, \frac{\sin\left(\frac{\pi}{\Delta X}(y - n\Delta X - y_{low})\right)}{\frac{\pi}{\Delta X}(y - n\Delta X - y_{low})}\, ds && (6.6)\\
&= \sum_{m=0}^{M-1}\sum_{n=0}^{N-1} g_d(m,n)\; K(\rho,\theta,m,n) && (6.7)\\
x &= \rho\cos\theta - s\sin\theta && (6.8)\\
y &= \rho\sin\theta - s\cos\theta && (6.9)
\end{aligned}$$

The kernel $K(\rho, \theta, m, n)$ is a integral, which can be rewritten into a convolution.

$$\left.\begin{aligned}
\alpha &= \tfrac{\pi}{\Delta X}(\rho\cos\theta - m\Delta X - x_{low})\\
\beta &= \tfrac{\pi}{\Delta X}(\rho\sin\theta - n\Delta X - y_{low})\\
\lambda &= \tfrac{\pi}{\Delta X}\cos\theta\\
\gamma &= \tfrac{\pi}{\Delta X}\sin\theta
\end{aligned}\right\} \Rightarrow K(\rho,\theta,m,n) = \int_{-\infty}^{\infty} \frac{\sin(\alpha - \gamma s)}{\alpha - \gamma s}\frac{\sin(\beta - \lambda s)}{\beta - \lambda s}\, ds \tag{6.10}$$

$$\left.\begin{aligned}
t &= \alpha - \gamma s\\
\kappa &= \tfrac{\lambda}{\gamma}\\
\phi &= \alpha + \tfrac{\beta}{\kappa}
\end{aligned}\right\} \Rightarrow K(\rho,\theta,m,n) = \frac{1}{|\gamma|}\int_{-\infty}^{\infty} \frac{\sin(t)}{t}\frac{\sin(\kappa(\phi - t))}{\kappa(\phi - t)}\, dt \tag{6.11}$$

$$= \frac{\pi}{|\gamma\kappa|}\frac{\sin(\phi\min\{1, |\kappa|\})}{\phi} \tag{6.12}$$

$$\Psi = \frac{\pi}{\Delta X}(\rho - x_m\cos\theta - y_n\sin\theta) \Rightarrow K(\rho,\theta,m,n) = \Delta X \frac{\sin\left(\Psi\min\left\{\frac{1}{|\cos\theta|}, \frac{1}{|\sin\theta|}\right\}\right)}{\Psi} \tag{6.13}$$

The result is that the Radon transform of the function shown in Equation 6.4 is given by the following equation.

$$\breve{g}(\rho,\theta) = \sum_{m=0}^{M-1}\sum_{n=0}^{N-1} g_d(m,n)\ \Delta X \frac{\sin\left(\Psi \min\left\{\frac{1}{|\cos\theta|},\frac{1}{|\sin\theta|}\right\}\right)}{\Psi} \tag{6.14}$$

This can also be seen as a consequence of Equation B.25.

$$\begin{aligned}
g(x,y) &= \int_{-\infty}^{\infty}\int_{-\infty}^{\infty} \frac{\sin(x-x')}{x-x'}\frac{\sin(y-y')}{y-y'} \sum_{m=0}^{M-1}\sum_{n=0}^{N-1} g(m,n)\delta(x'-x_m)\delta(y'-y_n)\ dx'dy' && (6.15)\\
&= \sum_{m=0}^{M-1}\sum_{n=0}^{N-1} g(m,n)\delta(x-x_m)\delta(y-y_n)\ **\ \frac{\sin(x)}{x}\frac{\sin(y)}{y} \ \Rightarrow && (6.16)\\
\breve{g}(\rho,\theta) &= \sum_{m=0}^{M-1}\sum_{n=0}^{N-1} g(m,n)\delta(\rho - x_m\cos\theta - y_n\sin\theta)\ *\ \Delta X \frac{\sin\left(\frac{\pi}{\Delta X}\rho \min\left\{\frac{1}{|\cos\theta|},\frac{1}{|\sin\theta|}\right\}\right)}{\frac{\pi}{\Delta X}\rho} && (6.17)
\end{aligned}$$

Equation 6.17 or 6.14 shows some fundamental limitations on the dynamics of the Radon transform. For instance is it possible to predict an adequate sampling in the ρ. If θ is fixed then Equation 6.14 shows that the upper limit frequency in the Radon domain is

$$\Delta\rho = \frac{1}{2\nu_{\max}} = \min_{\theta}\left\{\frac{\pi}{\frac{\pi}{\Delta X}\min\left\{\frac{1}{|\cos\theta|},\frac{1}{|\sin\theta|}\right\}}\right\} = \frac{\Delta X}{\sqrt{2}} \tag{6.18}$$

A fundamental result is that if inversion of the Radon transform is done with some output image sampling ΔX, then some preprocessing (low pass filtering) is needed to insure that the upper limit frequency in the sinogram complies with the wanted ΔX. But it is important to remember that any numerical implementation will introduce noise, which can limit the value of the theoretical analysis.

Chapter 7

Numerical Implementation of the direct algorithms

Several authors discuss implementations of the presented inversion schemes, e.g., [24, 16, 15, 26]. Here implementation of Filtered Backprojection, Filtering after Backprojection and the Central Slice Theorem are shown. All of these algorithms are based on the Fourier transform, which is reviewed in the next subsection.

7.1 Using the FFT instead of Fourier Transformation

All of the presented algorithms use Fourier transformation. In practice FFT (Fast Fourier Transform) is used. The FFT which is a numerically efficient way to calculate the discrete Fourier transform (DFT), and the DFT is an approximation to the the continuous Fourier transform.

Assume the one dimensional signal $g_a(t)$ is sampled, $g_d(n) = g_a(n\Delta T)$, and the signal is periodical, i.e., $g_d(n) = g_d(n+N)$. In this case the Fourier transform can be approximated by the discrete Fourier transform (DFT)

$$G_a(f) = \int_{-\infty}^{\infty} g_a(t)\ e^{-j2\pi ft}\ dt \approx \Delta T \sum_{n=0}^{N-1} g_d(n)\ e^{-j2\pi mn/N} = G_d(m) \tag{7.1}$$

$G_d(m)$ will approximate the continuous spectrum $G_a\left(\frac{m}{N\Delta T}\right)$. This discrete spectrum is computed using the discrete Fourier transform (DFT) of $g(n)$ and normally computed by use of the FFT. Using the same approximation the inverse Fourier transform is approximated by

$$g_a(t) = \int_{-\infty}^{\infty} G_a(f)\ e^{j2\pi ft}\ df \approx \frac{1}{N\Delta T} \sum_{m=0}^{N-1} G_d(m)\ e^{j2\pi mn/N} = g_d(n) \tag{7.2}$$

This technique can easily be generalized to two or more dimensions. The inverse Fourier transform can also be computed using the FFT. Note that the discrete spectrum is also periodical with period N. This implies that the maximum absolute frequency corresponds to $m = N/2 \Rightarrow f = \frac{1}{2\Delta T}$, i.e., half the sampling frequency. The last half or the array corresponds to the negative frequencies.

Now the practical use of the FFT for implementation of the operator $\mathcal{F}_{p1}^{-}$ will be discussed. It is very important to note that the FFT takes an array $g(n),\ n = 0, 1, ..., N-1$ and a signal to be transformed could be $h_a(t),\ t = -Q\Delta T, -Q\Delta T + \Delta T, ..., 0, ..., Q\Delta T$, stored in an array $h(n) = h_a(t), t(n) = -Q\Delta T + n\Delta T$. The array $g(n)$ must be filled as shown on Figure 7.1.

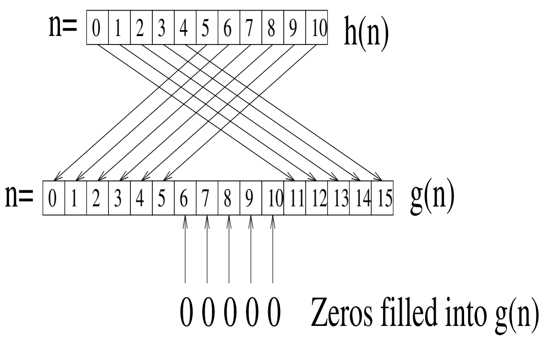

Figure 7.1: Filling an array $h(n)$ into a larger array $g(n)$, when using radix-2 FFT.

Note the wrapping so negative values of t are filled into the last half of the array. The zeros filled in the middle of the array serve two purposes. The zeros will affect the spectrum. A large number of zeros gives a smooth spectrum, which will relax the need for interpolation. Thus the extra zeros padded can help to improve the numerical stability. On Figure 7.2 a square signal is shown in the left upper corner, and the corresponding spectrum in the right upper corner. Zeros have been padded, and the spectrum has been found. This is shown on the lower part of the Figure. Note that the new spectrum is smoother.

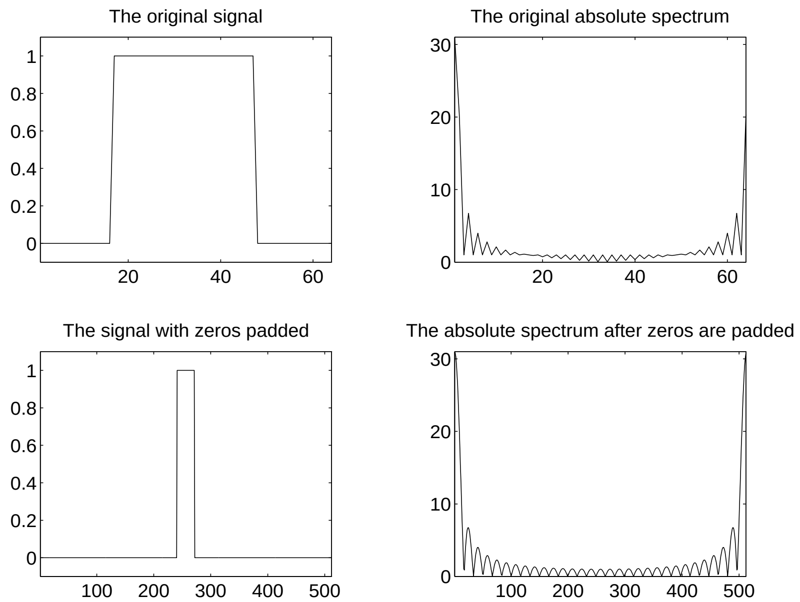

Figure 7.2: Zeros padded at the ends will smooth the spectrum.

Several effects must be noted when using FFT instead of the continuous Fourier transform. The spectrum is only available in discrete points. If the spectrum is needed in points between two discrete points, then interpolation must be used. The easiest method is the nearest neighbor strategy, which introduces numerical noise, but is fast. A better strategy is linear interpolation, where interpolation is used between the two nearest samples.

$$t_1 < t < t_2 \Rightarrow g(t) \approx \frac{(t_2 - t)g(t_1) + (t - t_1)g(t_2)}{t_2 - t_1} \tag{7.3}$$

The optimum interpolation is performed using a sinc-window. This can be implemented efficiently [26], but will imply a higher computational cost.

Another property, which can be used to reduce the computational cost is based on real signals. This can be used here because the Radon transform normally will be used images (without complex values).

Assume a discrete N-periodical one dimensional real sequence $g(n)$, then $G(m) = G(-m)^* = G(N-m)^*$, where * denotes the complex conjugate. This symmetry is easily proved from the DFT definition [21], and it should be used if only one real signal is transformed.

Numerical algorithms and program are available, e.g., from Numerical Recipes[1] to calculate the DFT of a real valued sequence $g(n)$ of length N. [2]

Normally the FFT-algorithm is a radix-2 algorithm, i.e., the transformation length must be a power of two. This restriction is in practice not harsh, but must be remembered when zeros are padded.

If an image (with real values) is to be transformed a similar symmetry can be used.

$$\begin{aligned}
g(m,n) &= g(m+M,n) = g(m,n+N) & (7.4)\\
G(u,v) &= \sum_{m=0}^{M-1}\sum_{n=0}^{N-1} g(m,n)\; e^{-j2\pi(mu/M+nv/N)} & (7.5)\\
G(u,v) &= G(m+M,n) = G(m,n+N) & (7.6)\\
g(m,n) &= g(m,n)^* \;\Rightarrow\; G(u,v) = G(-u,-v)^* = G(M-u,N-v)^* & (7.7)
\end{aligned}$$

This is shown on Figure 7.3.

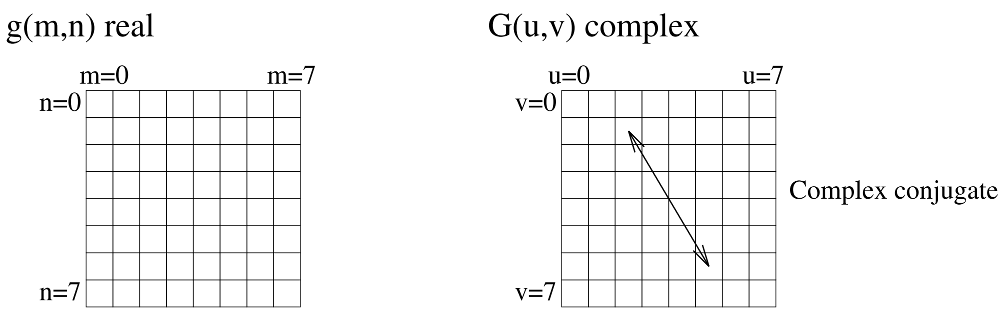

Figure 7.3: A real valued image gives a spectrum with complex conjugate pairs

7.2 Filtered Backprojection

Filtered Backprojection is the easiest inversion scheme to implement. An algorithm based on Filtered Backprojection will have two parts: A filtering part and an integration part[3]

- Filtering
  - For each t, i.e., θ calculate the discrete spectrum with respect to r (ρ) using FFT.

[1] See the functions REALFT.C and FOUR1.C, described in [9]

[2] Note that these programs use a special way to store the spectrum. Only the first half of the spectrum is returned in the array $g(n)$, and the two first positions of the array is special, due to that $G(0)$ and $G(N/2)$ are real. In the array $g(n)$ returned from the FFT is $g(0) = \mathrm{Re}(G(0))$, $g(1) = \mathrm{Re}(G(N/2))$, $g(2i) = \mathrm{Re}(G(i))$ and $g(2i+1) = \mathrm{Im}(G(0))$, $i = 1, 2, ...N/2-1$. This is very important.

[3] Assume that discrete values of the Radon transform of $g_d(m,n)$, i.e., $R_d(t,r)$ are given, and the zero padding and signal moving discussed in section 7.1 have been carried out.

- For each t, multiply with the filter ν, truncated at half of the sampling frequency and periodically repeated. This gives a filter, which is a sampled version of ν. Note that the last half of the array containing the filter corresponds to the negative frequencies.
- For each t, calculate the inverse discrete spectrum. Note that the result can be stored in the same matrix $R(t, r)$.

- Backprojection
  - The adjoint Radon transform can be approximated by a sum

$$g_d(m,n) = \Delta\theta \sum_{t=0}^{T-1} R(t, r_{t,m,n}) \tag{7.8}$$

Here $r_{t,m,n}$ is a function, which gives the value of r corresponding to x_m, y_n and θ_t cf. Equation 5.10. Note that here a nearest neighbor interpolation is implied, but better interpolation strategies can easily be incorporated.

The implementation of the function $r_{t,m,n}$ is rather important as optimization can improve the computational cost drastically.

$$\rho_r = r\Delta\rho + \rho_{min} = x_m \cos\theta_t + y_n \sin\theta_t \Rightarrow \tag{7.9}$$

$$r_{opt} = \frac{x_m}{\Delta\rho}\cos\theta_t + \frac{y_n}{\Delta\rho}\sin\theta_t - \frac{\rho_{min}}{\Delta\rho} \tag{7.10}$$

The optimal value of r, i.e., r_{opt} can be implemented as

- Compute the vectors xrel$[m] = \frac{x_m}{\Delta\rho}$, yrel$[n] = \frac{y_n}{\Delta\rho}$ and the constant roff $= \frac{\rho_{min}}{\Delta\rho}$.
- Compute the vectors costheta$[t] = \cos(\theta_t)$ and sintheta$[t] = \sin(\theta_t)$.
- Compute the matrices xc$[m,t] =$ xrel$[m] \cdot$ costheta$[t]$ and ys$[n,t] =$ yrel$[n] \cdot$ sintheta$[t] -$ roff.
- Using the definitions given above then $r_{opt} =$ xc$[m,t] +$ ys$[n,t]$. Note that the implementation can be optimized further if the matrices xc$[m,t]$ and ys$[n,t]$ can be programmed using the pointer to pointer technique.

The calculation of the cosine table can be optimized further using the recursive formula $\cos(x_{m+1}) = \cos x_m \cos\Delta X - \sin x_m \sin\Delta X$, but the finite precision of the computers imply that errors will build up. The given implementation of the r_{opt} shown above will only require two matrices and the computational load is lowered significantly.

Another strategy when implementing the r_{opt} is to use that ρ can be written as $\tilde{\rho}_{m,n}\cos(\theta_t + \tilde{\theta}_{m,n})$, where $x_m + jy_n = \tilde{\rho}_{m,n}e^{j\tilde{\theta}_{m,n}}$. This strategy implies that a table of cosine is needed, but multiplications are needed and rounding in the table is necessary.

7.3 Filtering after Backprojection

The backprojection part of this inversion algorithm is shown in subsection 7.2. After the backprojection the matrix $g_d(m,n)$ must be high pass filtered cf. Equation 4.33. Normally the spectrum has to be calculated using a one dimensional FFT. This is possible because the discrete spectrum can be written

$$G_d(u,v) = \sum_{m=0}^{M-1}\sum_{n=0}^{N-1} g_d(m,n)\ e^{-j2\pi(mu/M+nv/N)} \tag{7.11}$$

$$= \sum_{m=0}^{M-1}\left[\sum_{n=0}^{N-1} g_d(m,n)\ e^{-j2\pi mu/M}\right]\ e^{-j2\pi nv/N} \tag{7.12}$$

Note that both M and N must be powers of two if using a radix-2 FFT. If this is not true pad extra image points at the edges. The 2D-filtering is very easy, if the spectrum is calculated properly. It is possible to exploit the complex conjugate symmetry shown on Figure 7.3, but storage of the spectrum in the same matrix (possibly) will be odd. An easy strategy is to define a complex matrix and calculate the two dimensional DFT by use of two one dimensional DFT's. The complex spectrum can easily be multiplied by a sampled version of the filter $\sqrt{\sigma^2+\gamma^2}$.

$$\sigma \rightarrow \frac{u}{M\Delta X} \text{ and } \gamma \rightarrow \frac{v}{N\Delta Y} \tag{7.13}$$

$$\sqrt{\sigma^2+\gamma^2} \rightarrow \sqrt{\left(\frac{u}{M\Delta X}\right)^2+\left(\frac{v}{N\Delta Y}\right)^2} \tag{7.14}$$

If addressing the negative frequencies $\sigma < 0$, u must be replaced by $u - M$ and if $\gamma < 0$, v must be replaced by $v - N$. Symmetry can be used so approximately half of the complex spectrum is multiplied with the filter and the other half is duplicated from the first due to the complex conjugate symmetry. After the filtering is the inverse two dimensional DFT done, and the real part of the result is the discrete inversion of the Radon transform[4].

7.4 The Central Slice Theorem

The polar spectrum is calculated as shown in section 7.2. This spectrum must be mapped onto a rectangular grid, as shown on Figure 7.4.

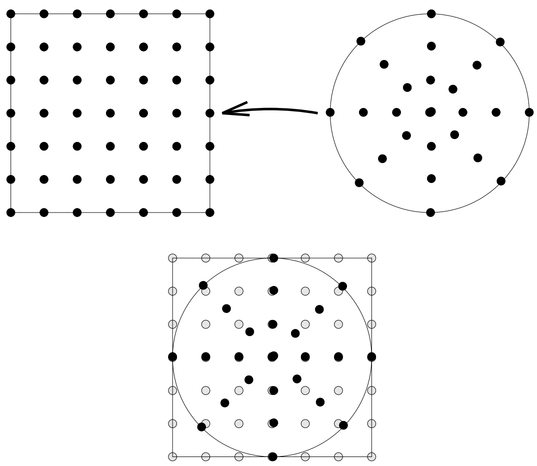

Figure 7.4: The polar and the rectangular spectrum.

If omitting the shifting problems discussed in chapter 7, the polar spectrum and and rectangular spectrum can match in three different ways as shown on Figure 7.5. The boundary corresponds to

[4]The imaginary part should be zero!

the maximum frequencies (half of the sampling frequencies). Note that $M = N$, $x_{min} = y_{min}$ and $\Delta X = \Delta Y$ is assumed.

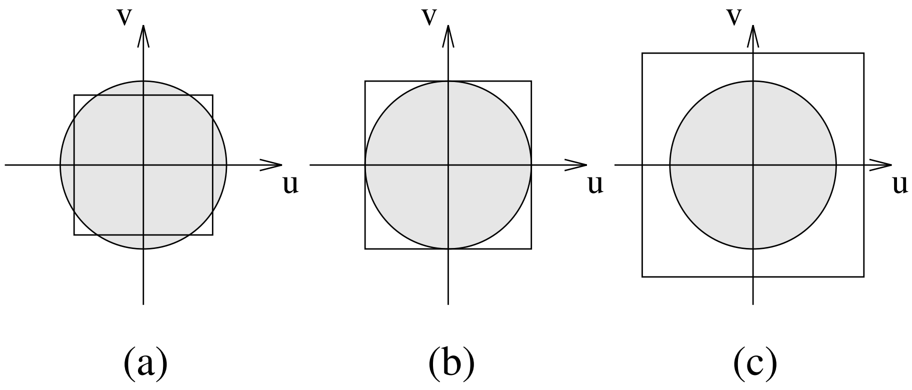

Figure 7.5: Three ways that the polar and the rectangular spectrum can match

In the first case (a) the rectangular spectrum is too small. Some of the polar spectrum is not mapped onto the rectangular spectrum. This is a very bad situation, and the result is unreliable. It will happen if $\sigma_{max} = \frac{1}{2\Delta X} < \nu_{max} = \frac{1}{2\Delta\rho}$, i.e., if $\Delta X > \Delta\rho$. In the second case (b) all of the polar spectrum is mapped onto the rectangular spectrum. This will happen when $\Delta X = \Delta\rho$. In the final case (c) The polar spectrum is less than the rectangular spectrum. This means that the output image will be low pass filtered. The sampling of the output image must also be smaller to adjust to the level of information in the polar spectrum. Note that the mapping from the polar spectrum onto the rectangular spectrum requires two dimensional interpolation. This will introduce much more numerical noise then accumulated in the backprojection algorithms. Especially the high frequencies are problematic, which implies that edges in the images are blurred. The problem can be reduced by use of high-order interpolation and/or use of a e.g. non-linear grid in the Radon domain.

7.4.1 Non-linear sampling of the Radon domain

The two dimensional interpolation in the frequency domain is problematic. This problem can be reduced by using a nonlinear grid in the Radon domain. The basic idea is to use a one dimensional interpolation in the frequency domain and (perhaps) an one dimensional interpolation in the Radon domain.

The last half of the Central Slice Theorem, i.e. the operator $\mathcal{F}_{2r}^{+}$ is easily implemented using rectangular sampling of the frequency domain. Thus the spectrum $G(k_x, k_y)$ is approximated by the two dimensional DFT $G_d(m, n)$ on a rectangular grid.

$$k_x = \frac{m}{M\Delta X} \tag{7.15}$$

$$k_y = \frac{n}{M\Delta X} \tag{7.16}$$

assuming $M = N$ and $\Delta X = \Delta Y$. The polar spectrum $H(\nu, \theta)$ is mapped onto the rectangular grid.

$$H(\nu, \theta) = G(k_x, k_y) \tag{7.17}$$

$$\begin{pmatrix} k_x \\ k_y \end{pmatrix} = \nu \begin{pmatrix} \cos\theta \\ \sin\theta \end{pmatrix} \tag{7.18}$$

If linear sampling of θ is applied, then the sampling of $\nu = r/(R\Delta\rho)$ can be chosen to vary with θ. The frequency plane is divided into two sectors where the available values of k_x and k_y are used

- Sector 1

$$
\begin{aligned}
0 \leq \theta < \frac{\pi}{4} \quad &\vee \quad \frac{3\pi}{4} \leq \theta < \pi && (7.19)\\
k_x \quad &= \quad \nu \cos\theta \Rightarrow && (7.20)\\
\nu \quad &= \quad \frac{k_x}{\cos\theta} = \frac{m}{M\Delta X \cos\theta} \Rightarrow && (7.21)\\
\Delta\nu \quad &= \quad \frac{1}{M\Delta X \cos\theta} && (7.22)
\end{aligned}
$$

- Sector 2

$$
\begin{aligned}
\frac{\pi}{4} < \quad &\theta \quad < \frac{3\pi}{4} && (7.23)\\
k_y \quad &= \quad \nu \sin\theta \Rightarrow && (7.24)\\
\nu \quad &= \quad \frac{k_y}{\sin\theta} \Rightarrow && (7.25)\\
\Delta\nu \quad &= \quad \frac{1}{M\Delta X \sin\theta} && (7.26)
\end{aligned}
$$

With this choise only one-dimensional interpolation of the spectrum is needed. The non-linear sampling of ν results in a non-linear sampling of ρ, i.e.

$$
\begin{aligned}
0 \leq \theta < \frac{\pi}{4} \vee \frac{3\pi}{4} \leq \theta < \pi \quad &\Rightarrow \quad \Delta\rho = \frac{M}{R}\Delta X \cos\theta && (7.27)\\
\frac{\pi}{4} < \theta < \frac{3\pi}{4} \leq \theta < \pi \quad &\Rightarrow \quad \Delta\rho = \frac{M}{R}\Delta X \sin\theta && (7.28)
\end{aligned}
$$

On Figure 7.6 is shown the non-linear sampling of the frequency domain, and Figure 7.7 shows the non-linear sampling of the Radon domain.

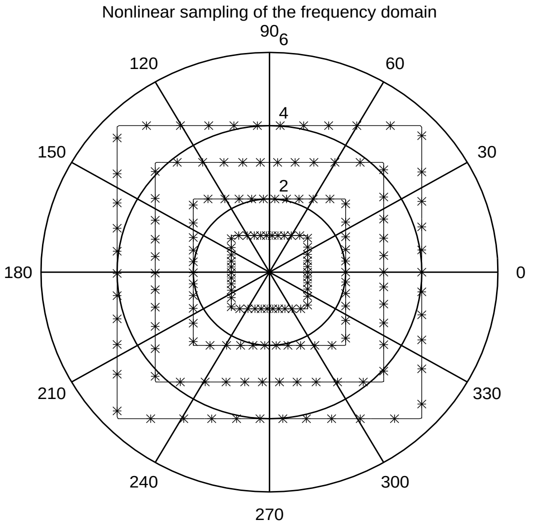

Figure 7.6: Non-linear sampling of the frequency domain.

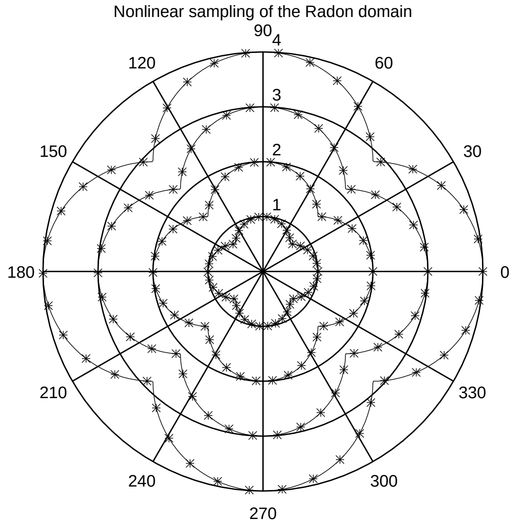

Figure 7.7: Non-linear sampling of the Radon domain.

If this technique is used only interpolation with respect to k_y is needed when $0 \leq \theta < \frac{\pi}{4} \vee \frac{3\pi}{4} \leq \theta < \pi$ and only with respect to k_x when $\frac{\pi}{4} < \theta < \frac{3\pi}{4}$. The additionel interpolation in the Radon domain is normally no critical because the Radon transform has low pass characteristics. Low-order interpolation is normally sufficient.

7.5 Additional Notes

In the previous chapters several inversion schemes have been presented. The major difference between the Central Slice Theorem based inversion and the Filtered Backprojection algorithms is speed and precision. Filtered Backprojection is normally precise but somewhat slow, with complexity $O(N^3)$, where N is the number of samples in one direction of the resulting image. Filtered Backprojection is the algorithm used in most scanners today. The Central Slice Theorem gives a fast algorithm, $O(N^2 \log N)$,but does not have the same numerical stability, due to the two-dimensional interpolation. Another promising algorithm is a hybrid between the two inversion schemes: *the Linogram Method*, see [15, 7]. This inversion method gives better numerical stability than implementations of the Central Slice Theorem and has complexity $O(N^2 \log N)$. The algorithm uses the non-linear sampling of the frequency domain described above.

The current trend aims to use one 3D inversion algorithm instead of using 2D inversion algorithm on a large number of individual slices. In PET this should make better use of the photons, and a realistic hope is that the dosage of the radioactive β^+-emitter could be lowered, when using 3D inversion algorithms. Several algorithms have been developed, based on Filtered Backprojection [5] and the linogram method [1].

Chapter 8

Inversion based on Linear Algebra

Discrete inversion of the Radon transform need not be based on the direct inverse formulas summerized in chapter 5. A radically different scheme is based on linear algebra [5].

Any discrete linear transformation can be written in a matrix vector formulation

$$\boldsymbol{b} = \boldsymbol{A}\boldsymbol{x} \tag{8.1}$$

where $\boldsymbol{b}$ is a B-dimensional vector, $\boldsymbol{x}$ a J-dimensional vector and $\boldsymbol{A}$ the transformation matrix. The Radon transform is a linear transform[1] and so is any discrete version of the Radon transform.

Assume a discrete set of values for the Radon transform $\breve{g}(\rho_r, \theta_t) = \breve{g}_d(r, t)$, and a given sampling of wanted image $g(x_m, y_n) = g_d(m, n)$ after discrete inversion. If the matrix $\breve{g}_d(r, t)$ is rearranged into a vector, e.g., $\boldsymbol{b}_{rT+t} = \breve{g}_d(r, t)$ and the same technique is applied to the image, e.g., $\boldsymbol{x}_{nM+m} = g_d(m, n)$, then the Radon transform can be written in the form shown in equation 8.1. The vector dimensions are $I = RT$ and $J = MN$, thus the transformation matrix $\boldsymbol{A}$ will normally we very large. The knowledge of the Radon transform makes it possible to find the matrix elements in $\boldsymbol{A}$, and another type of inversion could be based on equation 8.1. The straight forward inversion is simply

$$\boldsymbol{x} = \boldsymbol{A}^{-1}\boldsymbol{b} \tag{8.2}$$

and then the vector $\boldsymbol{x}$ could then be rearranged into the image $g_d(m, n)$. This inversion algorithm is very bad, because

- It turnes out that the structure of $\boldsymbol{A}$ is not regular, e.g. a band matrix, thus inversion of $\boldsymbol{A}$ must use rather slow methods.
- The matrix $\boldsymbol{A}$ is normally very large, e.g., 512^2 times 512^2 elements, thus inversion of $\boldsymbol{A}$ is very costly.
- The problem is ill-posed, i.e., several of the eigenvalues of $\boldsymbol{A}$ are equal to or very near zero. This implies that the system of equations in equation 8.1 cannot be solved without, e.g., regularization of equation system.

The matrix $\boldsymbol{A}$ can be estimated in various ways. One very common way, see e.g.[2], is to use a nearest neighbor approach. Around each pixel (x_m, y_m) is placed a square $\Delta X \times \Delta X$ wide. If the line with parameters (ρ_r, θ_t) crosses the square then the matrix element A_{ij} is set to 1. If not then to 0.

[1] with respect to the function $g(x, y)$

Note that this approach will not keep the correct normalization of the matrix elements. From Figure 8.1 it is easy to see that the test criterion can written as

$$\rho' = \rho_r - x_m \cos\theta_t - y_n \sin\theta_t \tag{8.3}$$

$$|\rho' \cos\theta_t| < \frac{\Delta X}{2} \quad \wedge \quad |\rho' \sin\theta_t| < \frac{\Delta X}{2} \;\Rightarrow\; A_{ij} = 1 \tag{8.4}$$

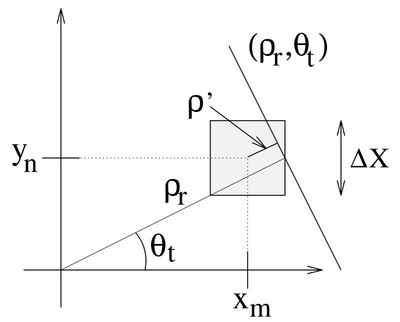

Figure 8.1: The line crosses the square pixel.

Another approach is to use Equation 6.14. Here a sinc interpolation scheme is used with the correct normalization. This expression gives the elements of the $\boldsymbol{A}$-matrix.

$$A_{ij} = \frac{\Delta X}{\Psi} \sin\left(\Psi \min\left\{\frac{1}{|\sin\theta_t|}, \frac{1}{|\cos\theta_t|}\right\}\right) \tag{8.5}$$

$$\Psi = \frac{\pi}{\Delta X}\left(\rho_r - x_m \cos\theta_t - y_n \sin\theta_t\right) \tag{8.6}$$

$$i = rT + t \quad \text{and} \quad j = nM + m \tag{8.7}$$

The last two equations can easily be inverted to give, e.g., r and t from a given value of i using truncation to lower integer and the modulus operator.

To illustrate the problems with inverting the matrix $\boldsymbol{A}$ calculated from Equation 8.5 a given set of sampling parameters has been chosen as shown in table 8.1. The corresponding matrix $\boldsymbol{A}$ is shown on Figure 8.2.

x_m	$=$	$-0.5 + m \cdot 0.05,$	$m = 0, 1, ..., 20$
y_n	$=$	$-0.5 + n \cdot 0.05,$	$n = 0, 1, ..., 20$
ρ_r	$=$	$-0.1 + r \cdot 0.1,$	$r = 0, 1, ..., 21$
θ_t	$=$	$t \cdot \frac{\pi}{20},$	$t = 0, 1, ..., 20$

Table 8.1: Parameter settings for the example.

The matrix $\boldsymbol{A}$ can be analysed by use of the SVD (Singular Value Decomposition) [13, 11, 17]. The basic idea of the SVD is to decompose the the matrix $\boldsymbol{A}$ as

$$\boldsymbol{A} = \boldsymbol{U}\boldsymbol{\Sigma}\boldsymbol{V}^T \tag{8.8}$$

where the matrix $\boldsymbol{\Sigma} \in \mathcal{R}^{I\times J}$ is a diagonal matrix with the singular values on the diagonal, $\boldsymbol{\Sigma} = \text{diag}(\sigma_1, \sigma_2, ..., \sigma_J)$ and the matrices $\boldsymbol{U} \in \mathcal{R}^{I\times I}$ and $\boldsymbol{V} \in \mathcal{R}^{J\times J}$ are orthonormal matrices. The singular

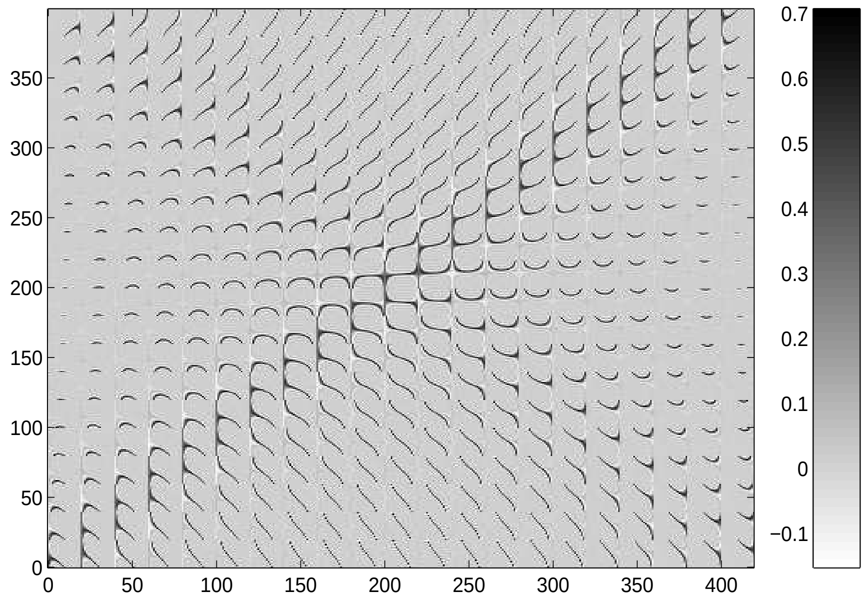

Figure 8.2: The $\boldsymbol{A}$-matrix

values are normally ordered in a non-increasing order, $\sigma_i \geq \sigma_{i+1}$, and the condition number of $\boldsymbol{A}$ is the ratio between the higest and the lowest singular value.

$$\mathrm{cond}(\boldsymbol{A}) = \frac{\sigma_1}{\sigma_J} \tag{8.9}$$

The singular values corresponding to the set of parameters is shown on Figure 8.3

From the Figure it can be seen that the problem is ill-posed. This is normally mended by restricting the variations of $\boldsymbol{x}$, by use of regularization, see e.g., [11].

8.1 Generalized Inversion using SVD

One way to invert an ill-posed problem is to formulate the inverse problem using that the last singular values are very small is to seperate the matrix $\boldsymbol{\Sigma}$ in a part with high singular values $\boldsymbol{\Sigma}_1$ and a part with low singular values $\boldsymbol{\Sigma}_2$.

$$\boldsymbol{\Sigma} = \begin{bmatrix} \boldsymbol{\Sigma_1} & \boldsymbol{0} \\ \boldsymbol{0} & \boldsymbol{\Sigma_2} \end{bmatrix} \tag{8.10}$$

where the singular values in $\boldsymbol{\Sigma}_2$ are insignificant. In this case the separation can be done choosing a rank p approximation, i.e. $\boldsymbol{\Sigma}_1 \in \mathcal{R}^{p\times p}$. The generalized inverse of $\boldsymbol{\Sigma}$ is defined as

$$\boldsymbol{\Sigma}^{-1} = \begin{bmatrix} \boldsymbol{\Sigma_1}^{-1} & \boldsymbol{0} \\ \boldsymbol{0} & \boldsymbol{0} \end{bmatrix} \tag{8.11}$$

Note that this inversion is easy to compute. The generalized inverse can be used for inversion of Equation 8.1.

$$\boldsymbol{x} = \boldsymbol{V}\boldsymbol{\Sigma}^{-1}\boldsymbol{U}^T\boldsymbol{b} \tag{8.12}$$

After the use of SVD the inversion can easily be found using matrix multiplications and the rank of $\boldsymbol{A}$ is easily incorporated in the inversion scheme. The suggested inversion strategy is not viable because

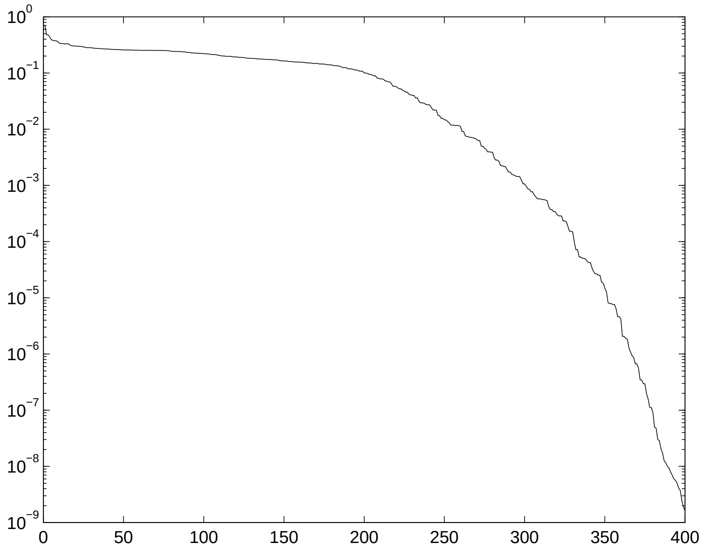

Figure 8.3: The singular values of the matrix $\boldsymbol{A}$.

SVD has complexity $\mathcal{O}(4I^2J+8IJ^2+9J^3)$, cf. [10], where m and n is the number of rows and columns of the matrix $\boldsymbol{A}$ respectively. This implies that the SVD used for inversion of the Radon transform has complexity approximately $\mathcal{O}(M^6)$. The SVD is still is very powerful tool to analyze the structure of the inverse problem.

Note that the presented technique can also be used for inversion of the nonlinear or generalized Radon transform. Another application of the technique is within three dimensional reconstruction in PET. If the two emitted photons can be detected in (virtually) all angles in a three dimensional space, i.e., the defined line is not restricted to be in a plane as previously, then the described linear algebra technique is applicable.

8.2 Inversion using ART

An traditional way to try to solve Equation 8.1 is named Algebraic Reconstruction Technique (ART). Many articles, see e.g. [2, 12, 13] shows the algorithm. Using the definition that the scalar product between to vectors $\boldsymbol{A}_i$ and $\boldsymbol{f}$ is

$$\sum_{j=0}^{J} A_{ij}\ x_j =< \boldsymbol{A}_i, \boldsymbol{x} > \tag{8.13}$$

then ART can be formulated as an iterative formula

$$\boldsymbol{x}^{(k+1)} = \boldsymbol{x}^{(k)} + \frac{b_i - < \boldsymbol{A}_i, \boldsymbol{x}^{(k)} >}{< \boldsymbol{A}_i, \boldsymbol{A}_i >} \boldsymbol{A}_i \tag{8.14}$$

ART is first published in the biomedical litterature in 1970. Later it was realized that the algorithm was introduced by Kaczmarz [14] in 1937.

Conventionally, see [13] i is chosen to $i = k$ MOD I, where MOD is the modulus operator, but this choise not optimal see [12]. Another strategy is to choose i randomly between 0 and I. Initially $\boldsymbol{x}^{(0)}$ can be chosen to zero or some good guess on the solution, e.g., in 2D from a fast algorithm like one based on Central Slice Theorem.

The main idea of ART if the equation i is fulfilled in iteration k. This is easily shown.

$$< \boldsymbol{A}_i, \boldsymbol{x}^{(k+1)} >=< \boldsymbol{A}_i, \boldsymbol{x}^{(k)} > + \frac{b_i - < \boldsymbol{A}_i, \boldsymbol{x}^{(\boldsymbol{k})} >}{< \boldsymbol{A}_i, \boldsymbol{A}_i >} < \boldsymbol{A}_i, \boldsymbol{A}_{\boldsymbol{i}} >= b_i \tag{8.15}$$

If using the Radon transformation terminology, then ART will modify the reconstructed image in iteration k, in order to give the correct Radon transform at (ρ_r, θ_t), where (r, t) is given from i. In this way the ART can produce better quality in a given area by choosing frequently that i matches the lines passing through the interesting area.

ART is very easy to implement, and a significant speedup can be found if truncating all alements in $\boldsymbol{A}$ below $\alpha \Delta X$ to zero, where $0 < \alpha < 1$. If α is chosen sufficiently low a good compromise between good resolution and a sparse matrix. Note that the sparse structure of $\boldsymbol{A}$ can efficiently be exploited when calculating the sums.

Chapter 9

Probabilistic Analysis of the PET scanning process

In the previous chapters the measured array of emissions cf. Equation 3.1 was assumed to be a stationary well defined function. This is not true. The emission intensity for a given set of ρ and θ is normally low, so the statistical behavior of the sinogram should be incorporated in the reconstruction process. If the attenuation correction is neglected (due to Equation 3.16) then the total number of double photon counts $E(\rho, \theta, \tau_e)$ follows a Poisson distribution. See, e.g., [20].

9.1 The Poissson Process

The distribution of a stochastic variable $\mathcal{X}$ following a Poisson distribution ($\mathcal{X} \in P(\lambda)$) is given by

$$P\{\mathcal{X} = k\} = \frac{\lambda^k}{k!} e^{-\lambda}, \;\; k \in N_0 \tag{9.1}$$

From the Poisson distribution it is found that

$$\begin{aligned} \mathrm{E}\{\mathcal{X}\} &= \lambda && (9.2) \\ \mathrm{V}\{\mathcal{X}\} &= \lambda && (9.3) \\ P\{\mathcal{X} = k\} &= P\{\mathcal{X} = k-1\} \; \frac{\lambda}{k} && (9.4) \end{aligned}$$

For PET usage the parameter λ is a function of the ρ and θ

$$\lambda = \lambda(\rho, \theta) = \check{I}(\rho, \theta) \; \tau_e \tag{9.5}$$

Note that $\check{I}(\rho, \theta)$ will not depend on τ_e if the decay of radioactive nuclei can be neglected.

From an ideal sinogram without noise, e.g., found analytically, the noise in the sinogram can be simulated as a function of time τ_e, using the Poisson process and histogram equalizing. Initially the sinogram is zero for all parameter values. Assume that a simulated sinogram $E_i(\rho, \theta)$ is wanted for $\tau_e = i \; \Delta\tau, \;\; i \in N$. For each parameter value the increment in the sinogram is a Poisson process.

$$E_{i+1}(\rho, \theta) = E_i(\rho, \theta) + \Delta E(\rho, \theta) \tag{9.6}$$

where

$$\Delta E(\rho, \theta) \in P(\lambda = \Delta\tau \; \check{I}(\rho, \theta)) \tag{9.7}$$

Normally an uniformly distributed variable x between 0 and 1 can be formed easily on a computer using the random number function[1]. For each time increment $\Delta\tau$ the Poisson distributed increment can be simulated using

$$\begin{aligned} W(k) &= P\{\Delta E(\rho,\theta) \leq k\} && (9.8) \\ \Delta E(\rho,\theta) &= W^{-1}(x) && (9.9) \end{aligned}$$

9.2 The Radon Transform and Noise

Noise is normally characterized by the autocorrelation.

$$R_h(x,y) = \int_{-\infty}^{\infty}\int_{-\infty}^{\infty} h(x',y')\ h(x-x',y-y')\ dx'\ dy' \tag{9.10}$$

Using Equation B.25 and B.9 with $\phi_0 = \pi$ is is possible to prodict (ideally) how noise will influence the reconstruction process [13, Section 10.8].

$$\begin{aligned} g(x,y) &= f(-x,-y) \ \Rightarrow && (9.11) \\ h(x,y) &= R_h(-x,-y) = f(x,y) ** g(x,y) && (9.12) \\ \check{h}(\rho,\theta) &= \check{f}(\rho,\theta) * \check{g}(\rho,\theta) = \int_{-\infty}^{\infty} \check{f}(\rho',\theta)\check{g}(\rho-\rho',\theta)\ d\rho' && (9.13) \\ &= \int_{-\infty}^{\infty} \check{f}(\rho',\theta)\check{f}(\rho'-\rho,\theta)\ d\rho' \ \Rightarrow && (9.14) \\ \mathcal{R}R_h(x,y) = \check{R}_h(\rho,\theta) &= \int_{-\infty}^{\infty} \check{f}(\rho',\theta)\check{f}(\rho'+\rho,\theta)\ d\rho' && (9.15) \\ &= R_{\check{h}}(\rho,\theta) && (9.16) \end{aligned}$$

This shows that the Radon transform of the autocorrelation of $h(x,y)$ is the one dimensional autocorrelation of the Radon transform of $h(x,y)$.

Assuming $\check{h}(\rho,\theta)$ is white and bandlimited noise for all θ up to ν_{max} then the noise power A_{rec} in the reconstructed function can be found.

$$\begin{aligned} \mathcal{F}_{p1}R_{\check{h}}(\rho,\theta) &\equiv S(\nu,\theta) = \begin{cases} A & |\nu| < \nu_{max} \\ 0 & |\nu| > \nu_{max} \end{cases} && (9.17) \\ A_{rec} &= R_h(0,0) = \int_{-\infty}^{\infty}\int_{-\infty}^{\infty} S(\sigma,\gamma)\ d\sigma\ d\gamma && (9.18) \\ &= \int_{-\infty}^{\infty}\int_{0}^{\pi} |\nu|\ S(\nu,\theta)\ d\nu\ d\theta && (9.19) \\ &= \pi A\nu_{max}^2 && (9.20) \end{aligned}$$

This is a very interesting result. The square power shows that the noise power in the reconstructed signal can be lowered with 6 db if ν_{max} can be lowered with at factor of two. If noise is a problem then the sinogram should be filtered along the ρ axis. The filtering would normally have a lowpass characteristic.

[1]See [9, Chapter 7] for a better way to generate random numbers

Chapter 10

Three Dimensional Inverse Radon Transformation

As mentioned in the last part of the previous chapter inversion of the three dimensional Radon transform can be used for recovery of the internal structure of a body described by plane integrals. The fundamental formulas based on the Radon transform are presented in the first sections. In the remaining part of the chapter lines in a three dimensional space are investigated. This geometry is important to three dimensional PET scanners, where the photon pairs not are restricted to define a set of equidistant planes as presented previously.

10.1 The Three Dimensional Radon Transformation

The general form of the Radon transformation in N dimensions is

$$\tilde{g}(\rho, \boldsymbol{\xi}) = \int_{-\infty}^{\infty} g(\boldsymbol{r})\ \delta(\rho - \boldsymbol{\xi} \cdot \boldsymbol{r})\ d\boldsymbol{r} \tag{10.1}$$

where $\boldsymbol{r}$ and $\boldsymbol{\xi} \in \boldsymbol{R}^N$ but $\boldsymbol{\xi}$ has only N-1 degrees of freedom, e.g., done by normalizing $|\boldsymbol{\xi}| = 1$. A common approach is to express the vector $\boldsymbol{\xi}$ in hyper-spherical coordinates [5, page 112]. In two dimensions $\boldsymbol{\xi} = (\cos\theta, \sin\theta)^T$ and in three dimensions the vector is normally chosen to

$$\boldsymbol{\xi} = \begin{pmatrix} \cos\phi \sin\theta \\ \sin\phi \sin\theta \\ \cos\theta \end{pmatrix} \tag{10.2}$$

The fundamental body of the Radon transform is in two dimensions a line and in three dimensions a plane described by the kernel of the Radon transform

$$\rho = x\cos\phi\sin\theta + y\sin\phi\sin\theta + z\cos\theta \ \Rightarrow \tag{10.3}$$

$$\breve{g}(\rho,\theta,\phi) = \int_{x=-\infty}^{\infty}\int_{y=-\infty}^{\infty}\int_{y=-\infty}^{\infty} g(\boldsymbol{r})\ \delta(\rho - x\cos\phi\sin\theta - y\sin\phi\sin\theta - z\cos\theta)\ dx\ dy\ dz \tag{10.4}$$

Here it can be noted that the three dimensional Radon transform will transform a three dimensional signal $g(\boldsymbol{r})$ into a three dimensional parameter domain $\breve{g}(\rho, \theta, \phi)$.

The three dimensional Radon transform can be viewed as a convolution with a filter

$$\delta(\boldsymbol{\xi}) \tag{10.5}$$

META Write more here

10.2 The Three Dimensional Fourier Slice Theorem

The Fourier Slice Theorem can also be generalized to the three dimensional case. The inversion formula is based on Fourier transformation of Equation 10.1.

$$\begin{aligned}
\check{G}(\nu, \boldsymbol{\xi}) &= \int_{-\infty}^{\infty} \check{g}(\rho, \boldsymbol{\xi})\ e^{-j2\pi\rho\nu}\ d\rho && (10.6)\\
&= \int_{-\infty}^{\infty} \left[\int_{-\infty}^{\infty} g(\boldsymbol{r})\ \delta(\rho - \boldsymbol{\xi}\cdot\boldsymbol{r})\ d\boldsymbol{r}\right]\ e^{-j2\pi\rho\nu} d\rho && (10.7)\\
&= \int_{-\infty}^{\infty} g(\boldsymbol{r})\ e^{-j2\pi\nu\boldsymbol{\xi}\cdot\boldsymbol{r}}\ d\boldsymbol{r} && (10.8)
\end{aligned}$$

Defining the frequency parameters being

$$\nu\boldsymbol{\xi} = \begin{pmatrix} u \\ v \\ w \end{pmatrix} \tag{10.9}$$

then the one dimensional Fourier transform of $\check{g}$ can be recognized to the three dimensional Fourier transform of g.

$$\begin{aligned}
\check{G}(\nu, \boldsymbol{\xi}) &= \int_{-\infty}^{\infty}\int_{-\infty}^{\infty}\int_{-\infty}^{\infty} g(x,y,z)\ e^{-j2\pi(xu+yv+zw)}\ dx\ dy\ dz \Leftrightarrow && (10.10)\\
g(r) = g(x,y,z) &= \int_{-\infty}^{\infty}\int_{-\infty}^{\infty}\int_{-\infty}^{\infty} \check{G}(\nu, \boldsymbol{\xi})\ e^{j2\pi(xu+yv+zw)}\ du\ dv\ dw && (10.11)
\end{aligned}$$

Note that the result is very similar to the two dimensional result and here the transformation is from a three dimensional domain into another three dimensional domain.

10.3 Filtered Backprojection in 3D

Filtered Backprojection can also be generalized into a 3D version. The inversion scheme is derived by expressing Equation 10.11 in spherical coordinates.

$$g(x,y,z) = g(\boldsymbol{r}) = \int_{\nu=0}^{\infty}\int_{\theta=0}^{\pi}\int_{\phi=0}^{2\pi} \nu^2 \sin\theta\ \check{G}(\nu, \boldsymbol{\xi})\ e^{j2\pi\nu\boldsymbol{\xi}\cdot\boldsymbol{r}}\ d\phi\ d\theta\ d\nu \tag{10.12}$$

Using that a real-valued $g(\boldsymbol{r})$ implies that the spectrum has a complex conjugate symmetry

$$\begin{aligned}
G(\boldsymbol{\nu}) &= G(-\boldsymbol{\nu})^* \ \Rightarrow && (10.13)\\
\check{G}(\nu, \boldsymbol{\xi}) &= \check{G}(\nu, \theta, \phi) = \check{G}(-\nu, \pi - \theta, \phi - \pi) && (10.14)
\end{aligned}$$

This is inserted in Equation 10.12

$$g(\boldsymbol{r}) = \int_{\nu=-\infty}^{\infty}\int_{\theta=0}^{\pi}\int_{\phi=0}^{\pi} \nu^2 \sin\theta\ \check{G}(\nu, \boldsymbol{\xi})\ e^{j2\pi\nu\boldsymbol{\xi}\cdot\boldsymbol{r}}\ d\phi\ d\theta\ d\nu \tag{10.15}$$

Now Equation 10.8 is inserted into Equation 10.15.

$$g(\boldsymbol{r}) = \int_{\nu=-\infty}^{\infty}\int_{\theta=0}^{\pi}\int_{\phi=0}^{\pi} \nu^2 \sin\theta\ \left[\int_{\rho=-\infty}^{\infty} \check{g}(\rho, \theta, \phi)\ e^{-j2\pi\nu\rho}\ d\rho\right]\ e^{j2\pi\nu\boldsymbol{\xi}\cdot\boldsymbol{r}}\ d\phi\ d\theta\ d\nu \tag{10.16}$$

This equation can for convenience be written in two parts

$$g^{\dagger}(\rho,\theta,\phi) = \sin\theta \int_{\nu=-\infty}^{\infty} \nu^2 \left[\int_{\rho=-\infty}^{\infty} \breve{g}(\tilde{\rho},\theta,\phi)\ e^{-j2\pi\nu\tilde{\rho}}\ d\tilde{\rho}\right] e^{j2\pi\nu\rho}\ d\nu \tag{10.17}$$

$$g(\boldsymbol{r}) = \int_{\theta=0}^{\pi}\int_{\phi=0}^{\pi} g^{\dagger}(\boldsymbol{\xi}\cdot\boldsymbol{r},\theta,\phi)\ d\phi\ d\theta \tag{10.18}$$

$$= \int_{\rho=-\infty}^{\infty}\int_{\theta=0}^{\pi}\int_{\phi=0}^{\pi} g^{\dagger}(\rho,\theta,\phi)\ \delta(\rho-\boldsymbol{\xi}\cdot\boldsymbol{r})\ d\phi\ d\theta\ d\rho \tag{10.19}$$

Note the similarity between the 2D Filtered Backprojection inversion scheme and the 3D version as shown in Equation 10.17 and 10.19. Naturally Equation 10.19 is named the adjoint Radon transform. Note also that the filtering part of 3D Filtered Backprojection requires a quadratic filter ν^2.

10.4 Lines in a Three Dimensional Space

Lines in a three dimensional space cannot be written in a single normal form as in the two dimensional case. Instead a parameter description can be used. In the following a line description using four parameters are shown. This description is the basis of a direct inversion scheme for lines in a three dimensional space. In general a line be described by

$$\boldsymbol{r} = \boldsymbol{r}_0 + t\boldsymbol{\tau} \tag{10.20}$$

Note that other symbols of the vectors can be found in the literature [17, 18, 19]. The vector $\boldsymbol{\tau}$ is a directional vector which can be normalized to unit length, i.e., $\boldsymbol{\tau} = 1$. The vector can, e.g., be described by

$$\boldsymbol{\tau} = \begin{pmatrix} \cos\theta\cos\phi \\ \sin\theta\cos\phi \\ \sin\phi \end{pmatrix} \tag{10.21}$$

The base point vector $\boldsymbol{r}_0$ is described by two parameters u and v using two directional vectors $\boldsymbol{\alpha}$ and $\boldsymbol{\beta}$ derived from $\boldsymbol{\tau}$.

$$\boldsymbol{r}_0 = u\boldsymbol{\alpha} + v\boldsymbol{\beta} \tag{10.22}$$

It can be chosen that the three vectors $\boldsymbol{\tau}$, $\boldsymbol{\alpha}$ and $\boldsymbol{\beta}$ form an orthonormal basis, and the last rotational degree of freedom can be used for specifying that the z-component of $\boldsymbol{\alpha}$ is zero. Different definitions of the vectors are found in the literature, e.g., [22] where $\boldsymbol{\alpha}$ and $\boldsymbol{\beta}$ are given by

$$\boldsymbol{\alpha} = \begin{pmatrix} -\sin\theta \\ \cos\theta \\ 0 \end{pmatrix} \text{ and } \boldsymbol{\beta} = \begin{pmatrix} -\cos\theta\sin\phi \\ -\sin\theta\sin\phi \\ \cos\phi \end{pmatrix} \tag{10.23}$$

Following [3], line integrals in a three dimensional space can be expressed by the symbols defined in Equation 10.20 and 10.22

$$\breve{g}(\theta,\phi,u,v) = \int_{-\infty}^{\infty} g(t\boldsymbol{\tau} + u\boldsymbol{\alpha} + v\boldsymbol{\beta})\ dt \tag{10.24}$$

The mapping from the (x, y, z) domain to (t, u, v) or principal component domain is important

$$\boldsymbol{r} = t\boldsymbol{\tau} + u\boldsymbol{\alpha} + v\boldsymbol{\beta} \Rightarrow \tag{10.25}$$

$$\boldsymbol{r} = \begin{pmatrix} x \\ y \\ z \end{pmatrix} = \begin{pmatrix} \cos\theta\cos\phi & -\sin\theta & -\cos\theta\sin\phi \\ \sin\theta\cos\phi & \cos\theta & -\sin\theta\sin\phi \\ \sin\phi & 0 & \cos\phi \end{pmatrix} \begin{pmatrix} t \\ u \\ v \end{pmatrix} = \boldsymbol{L}\boldsymbol{p} \tag{10.26}$$

Using that the base vectors are orthonormal implies that the rotation matrix $\boldsymbol{L}$ is unitary, hence

$$\boldsymbol{p} = \boldsymbol{L}^{-1}\boldsymbol{r} = \boldsymbol{L}^T\boldsymbol{r} \Rightarrow \tag{10.27}$$

$$\begin{pmatrix} t \\ u \\ v \end{pmatrix} = \begin{pmatrix} \cos\theta\cos\phi & \sin\theta\cos\phi & \sin\phi \\ -\sin\theta & \cos\theta & 0 \\ -\cos\theta\sin\phi & -\sin\theta\sin\phi & \cos\phi \end{pmatrix} \begin{pmatrix} x \\ y \\ z \end{pmatrix} \tag{10.28}$$

One very important feature with the matrix $\boldsymbol{L}$ is that it only uses two angles compared to a general rotation matrix with three degrees of freedom, i.e., three angles. The definition implies that a three dimensional function $g(x, y, z)$ is transformed into a four dimensional parameter domain $\breve{g}(\theta, \phi, u, v)$. This imposes some difficulties to be analyzed later. Here it is also chosen to denote the three dimensional line integral of $g(\boldsymbol{r})$ with the symbol $\breve{g}$. It can be argued that Equation 10.24 is not a Radon transform of the function g. It is not, cf. Equation 10.1, a three dimensional Radon transform nor a two dimensional, but it can be seen as a hybrid or generalized Radon transform for lines a a three dimensional space. In the following it is referred as the 3D line Radon transform or simply the Radon transform. The number of parameters will uniquely determine which type of transformation is used, and should not lead to confusion. From the definition of the 3D line Radon transform some basic rules are derived. These are shown in Appendix D. Additionally, the Radon transform of simple geometrical functions are given in the same appendix.

The 3D line Radon transform can be viewed as a convolution between a function $g(\boldsymbol{r})$ and a kernel expressed in the principal components $\boldsymbol{p}$ at a given combination of the angles θ and ϕ.

$$h(\boldsymbol{r}) = h(\boldsymbol{p}) = h(t, u, v) = \delta(u)\delta(v) \tag{10.29}$$

This can be seen from the following, where $***$ implies a three dimensional convolution in the parameters (t, u, v).

$$\begin{aligned} \breve{g}(\theta, \phi, u, v) &= g(\boldsymbol{r}) *** \delta(u)\delta(v) && (10.30) \\ &= \int_{v'=-\infty}^{\infty}\int_{u'=-\infty}^{\infty}\int_{t'=-\infty}^{\infty} g(t'\boldsymbol{\tau} + u'\boldsymbol{\alpha} + v'\boldsymbol{\beta})\ \delta(u-u')\delta(v-v')\ dt'\ du'\ dv' && (10.31) \\ &= \int_{t'=-\infty}^{\infty} g(t'\boldsymbol{\tau} + u\boldsymbol{\alpha} + v\boldsymbol{\beta})\ dt' && (10.32) \end{aligned}$$

Besides the new integration variable t' the result matches Equation 10.24. It can be seen that the 3D plane Radon transform is complementary to the 3D line Radon transform. They convolve opposite. META write more here

At this time it could be appropriate to look back to the two dimensional results. This can be done by choosing $\phi = 0$, $v = z_0$ and $u = \rho$. Thus the line integral reduces to

$$\breve{g}(\rho, 0, \theta) = \int_{-\infty}^{\infty} g(t\cos\theta - \rho\sin\theta, t\sin\theta + \rho\cos\theta, z_0)\ dt \tag{10.33}$$

From Equation 2.5 this can be recognized to be the ordinary two dimensional Radon transform of the function in the plane $z = z_0$, where the angular parameter θ has been rotated 90 degrees compared to the definition of the two dimensional Radon transform.

10.4.1 Limiting the 3D line parameters

It is quite obvious that the angular parameters θ and ϕ control the orientation of the line and they are bounded as normal, i.e., $0 \leq \theta < \pi$ and $-\pi/2 \leq \phi < \pi/2$. This corresponds to a full angular coverage.

In [3] three popular geometries are mentioned

$$\Omega_0 = \{0 \leq \theta < \pi \ \vee \ \phi = 0\} \tag{10.34}$$
$$\Omega_{\pi/2} = \{0 \leq \theta < \pi \ \vee \ -\pi/2 \leq \phi < \pi/2\} \tag{10.35}$$
$$\Omega_\psi = \{0 \leq \theta < \pi \ \vee \ |\phi| \leq \psi\} \tag{10.36}$$

Here Ω_0 corresponds to the two dimensional case treated in the previous chapters (see also Equation 10.33), $\Omega_{\pi/2}$ is full angular coverage and Ω_ψ is applicable in the truncated cylinder found in commercial 3D PET-scanners. META Find parameter bounds from formulas. Write later!

The two remaining parameters u and v are translation parameters controlling the position of the line. In theory they can only be bounded if it can be assumed that the scanned object is finite. The origin of the three dimensional coordinate system is placed (approximatively) at the center of the object. This implies that the distance from the origin to the outer edge of the object is minimized to $r_{\max}$, or with mathematical terms

$$g(x, y, z) = 0 \text{ for } x^2 + y^2 + z^2 > r_{\max}^2 \tag{10.37}$$

If $r_{\max}$ is found then u and v can be restricted, because the distance from the origin to the volume element at $\boldsymbol{r} = t\boldsymbol{\tau} + u\boldsymbol{\alpha} + v\boldsymbol{\beta}$ are $|\boldsymbol{r}| = \sqrt{t^2 + u^2 + v^2}$. This is due to othonormality of the three expansion vectors. Assuming that $u^2 + v^2 > r_{\max}^2$, implies that the integral is zero, because the volume elements are zero along the line. This very important result implies that each of the translation parameters can be bounded between $-r_{\max}$ and $r_{\max}$, i.e., the four parameters can be bounded choosing

$$0 \leq \theta < \pi \tag{10.38}$$
$$-\pi/2 \leq \phi < \pi/2 \tag{10.39}$$
$$-r_{\max} \leq u \leq r_{\max} \tag{10.40}$$
$$-r_{\max} \leq v \leq r_{\max} \tag{10.41}$$

10.5 Fourier Transform based Inversion of Line Integrals in a Three Dimensional Space

From the line integrals defined in Equation 10.24 the function $g(\boldsymbol{r})$ can be recovered using Fourier techniques. Analogously to the Fourier Slice Theorem is now derived by applying the two dimensional Fourier transform to Equation 10.24.

$$\check{G}(\theta, \phi, \nu_u, \nu_v) = \int_{-\infty}^{\infty}\int_{-\infty}^{\infty} \check{g}(\theta, \phi, u, v)\ e^{-j2\pi(u\nu_u + v\nu_v)}\ du\ dv \tag{10.42}$$
$$= \int_{-\infty}^{\infty}\int_{-\infty}^{\infty}\int_{-\infty}^{\infty} g(t\boldsymbol{\tau} + u\boldsymbol{\alpha} + v\boldsymbol{\beta})\ e^{-j2\pi(u\nu_u + v\nu_v)}\ du\ dv\ dt \tag{10.43}$$

This indicates a close connection to the three dimensional Fourier transform of the function $g(\boldsymbol{r})$.

$$G(\boldsymbol{\nu}) = \int_{-\infty}^{\infty}\int_{-\infty}^{\infty}\int_{-\infty}^{\infty} g(\boldsymbol{r})\ e^{-j2\pi\boldsymbol{r}\cdot\boldsymbol{\nu}}\ d\boldsymbol{r} \tag{10.44}$$
$$g(\boldsymbol{r}) = \int_{-\infty}^{\infty}\int_{-\infty}^{\infty}\int_{-\infty}^{\infty} G(\boldsymbol{\nu})\ e^{j2\pi\boldsymbol{r}\cdot\boldsymbol{\nu}}\ d\boldsymbol{\nu} \tag{10.45}$$

where $\boldsymbol{\nu}$ is the three dimensional frequency vector.

Now the integration parameters in Equation 10.43 is changed into x, y and z, i.e., $\boldsymbol{r}$. It is used that $\boldsymbol{\tau}$, $\boldsymbol{\alpha}$ and $\boldsymbol{\beta}$ form an orthonormal basis.

$$\boldsymbol{r} = t\boldsymbol{\tau} + u\boldsymbol{\alpha} + v\boldsymbol{\beta} \;\Rightarrow \tag{10.46}$$
$$u = \boldsymbol{\alpha}\cdot\boldsymbol{r} \;\text{ and }\; v = \boldsymbol{\beta}\cdot\boldsymbol{r} \;\Rightarrow \tag{10.47}$$
$$u\nu_u + v\nu_v = \boldsymbol{r}\cdot(\nu_u\boldsymbol{\alpha} + \nu_v\boldsymbol{\beta}) \Rightarrow \tag{10.48}$$
$$\check{G}(\theta,\phi,\nu_u,\nu_v) = \int_{-\infty}^{\infty}\int_{-\infty}^{\infty}\int_{-\infty}^{\infty} g(\boldsymbol{r})\; e^{-j2\pi\boldsymbol{r}\cdot(\nu_u\boldsymbol{\alpha}+\nu_v\boldsymbol{\beta})}\; d\boldsymbol{r} \tag{10.49}$$

This interesting result shows that the two dimensional Fourier transform of the the line integrals is the three dimensional Fourier transform of the function to be reconstructed.

$$\check{G}(\theta,\phi,\nu_u,\nu_v) = G(\nu_u\boldsymbol{\alpha} + \nu_v\boldsymbol{\beta}) \tag{10.50}$$

This can be seen as a Fourier Slice Theorem for line integrals in a three dimensional space. This implies that the function $g(\boldsymbol{r})$ can be recovered by applying a two dimensional Fourier transform and then a three dimensional inverse Fourier transform.

$$G(\nu_u\boldsymbol{\alpha} + \nu_v\boldsymbol{\beta}) = \int_{-\infty}^{\infty}\int_{-\infty}^{\infty} \check{g}(\theta,\phi,u,v)\; e^{-j2\pi(u\nu_u+v\nu_v)}\; du\; dv \tag{10.51}$$
$$g(\boldsymbol{r}) = \int_{-\infty}^{\infty}\int_{-\infty}^{\infty}\int_{-\infty}^{\infty} G(\boldsymbol{\nu})\; e^{j2\pi\boldsymbol{r}\cdot\boldsymbol{\nu}}\; d\boldsymbol{\nu} \tag{10.52}$$

A problem arises when implementing the algorithm. For each frequency point, $\boldsymbol{\nu}$ is set to $\nu_u\boldsymbol{\alpha} + \nu_v\boldsymbol{\beta}$. Note that $\boldsymbol{\nu}$ is a three-dimensional vector and $\nu_u\boldsymbol{\alpha}+\nu_v\boldsymbol{\beta}$ has four degrees of freedom. This implies that each $\boldsymbol{\nu}$ matches an infinite set of parameters θ,ϕ,u,v. META Investigate this. Why this problem. Relate to 4D -¿ 3D problem

10.6 Backprojection Based Inversion of Line Integrals in a Three Dimensional Space

Analogous to the two-dimensional Filtered Backprojection it is possible to filter the line projections and then make a backprojection [3]. The filtering can also be "moved" to the image domain like in the Filtering after backprojection algorithm. Here the backprojection part is analyzed from the transformation of a point source. Any function can be resolved into a weighted sum (integral) of delta functions.

$$g(\boldsymbol{r}) = \int_{-\infty}^{\infty}\int_{-\infty}^{\infty}\int_{-\infty}^{\infty} g(\boldsymbol{r}_0)\; \delta(x-x_0)\delta(y-y_0)\delta(z-z_0)\; dx_0\; dy_0\; dz_0 \tag{10.53}$$
$$\equiv \int_{-\infty}^{\infty} g(\boldsymbol{r}_0)\; \delta(\boldsymbol{r}-\boldsymbol{r}_0)\; d\boldsymbol{r}_0 \tag{10.54}$$

This implies that the corresponding Radon transform is given by

$$\check{g}(\theta,\phi,u,v) = \int_{-\infty}^{\infty} g(\boldsymbol{r}_0) \int_{t=-\infty}^{\infty} \delta(t\boldsymbol{\tau} + u\boldsymbol{\alpha} + v\boldsymbol{\beta} - \boldsymbol{r}_0)\; dt\; d\boldsymbol{r}_0 \tag{10.55}$$

This shows that any function $g(\boldsymbol{r})$ can be Radon transformed, if the point source can be transformed. This will now be analyzed.

$$g_p(\boldsymbol{r}) = \delta(\boldsymbol{r}-\boldsymbol{r}_0) \;\Rightarrow \tag{10.56}$$

$$
\begin{aligned}
\breve{g}_p(\theta,\phi,u,v) &= \int_{-\infty}^{\infty} \delta(t\boldsymbol{\tau} + u\boldsymbol{\alpha} + v\boldsymbol{\beta} - \boldsymbol{r}_0)\ dt && (10.57)\\
&= \int_{-\infty}^{\infty} \delta((t-t_0)\boldsymbol{\tau} + (u-u_0)\boldsymbol{\alpha} + (v-v_0)\boldsymbol{\beta})\ dt && (10.58)\\
&= \int_{-\infty}^{\infty} \delta(\tilde{t}\boldsymbol{\tau} + (u-u_0)\boldsymbol{\alpha} + (v-v_0)\boldsymbol{\beta})\ d\tilde{t} && (10.59)
\end{aligned}
$$

Here the unambiguous substitution $\boldsymbol{r}_0 = t_0\boldsymbol{\tau} + u_0\boldsymbol{\alpha} + v_0\boldsymbol{\beta}$ has been used. Using that the delta function will be nonzero iff the argument is a zero length vector implies that the result will be nonzero only if $u = u_0 = \boldsymbol{r}_0 \cdot \boldsymbol{\alpha}$ and $v = v_0 = \boldsymbol{r}_0 \cdot \boldsymbol{\beta}$. Using that the base vectors are orthogonal the result can be expressed using the delta function.

$$
\breve{g}_p(\theta,\phi,u,v) = \delta(u-u_0)\delta(v-v_0) = \delta(u-\boldsymbol{r}_0\cdot\boldsymbol{\alpha})\delta(v-\boldsymbol{r}_0\cdot\boldsymbol{\beta}) \qquad (10.60)
$$

This can also be found directly from Equation 10.30. It is a very important result which can be used to used to formulate a backprojection operator in 3D.

$$
\tilde{g} = \int_{\Omega} \breve{g}(\theta,\phi,u=\boldsymbol{r}\cdot\boldsymbol{\alpha}, v=\boldsymbol{r}\cdot\boldsymbol{\beta})\ d\Omega \qquad (10.61)
$$

For convenience the integration over angles is written as a single integral with index Ω. If the geometry is, e.g., Ω_ψ the integration becomes

$$
\int_{\Omega_\psi} f(\theta,\phi)\ d\Omega = \int_{\theta=0}^{\pi}\int_{\phi=-\psi}^{\psi} f(\theta,\phi)\ \cos\phi\ d\phi\ d\theta \qquad (10.62)
$$

10.7 Filtering after Backprojection for three dimensional lines

Like in two dimensional backprojection algorithms a high pass-filter is needed either before or after the backprojection [3]. In this section the aim is to find a condition for the post-processing filter. It can be derived be backprojecting the Radon transform. Inserting Equation 10.24 in 10.61 gives

$$
\tilde{g}(\boldsymbol{r}) = \int_{\Omega}\int_{t=-\infty}^{\infty} g((\boldsymbol{r}\cdot\boldsymbol{\alpha})\boldsymbol{\alpha} + (\boldsymbol{r}\cdot\boldsymbol{\beta})\boldsymbol{\beta} + t\boldsymbol{\tau})\ dt\ d\Omega \qquad (10.63)
$$

Now it is utilized that the t-integration can be shifted along the $\boldsymbol{\tau}$-axis, like it was done from Equation 10.58 to 10.59. Here the offset is chosen to $t_0 = \boldsymbol{r}\cdot\boldsymbol{\tau}$.

$$
\begin{aligned}
\tilde{g}(\boldsymbol{r}) &= \int_{\Omega}\int_{t=-\infty}^{\infty} g((\boldsymbol{r}\cdot\boldsymbol{\alpha})\boldsymbol{\alpha} + (\boldsymbol{r}\cdot\boldsymbol{\beta})\boldsymbol{\beta} + (\boldsymbol{r}\cdot\boldsymbol{\tau})\boldsymbol{\tau} + t\boldsymbol{\tau})\ dt\ d\Omega && (10.64)\\
&= \int_{\Omega}\int_{t=-\infty}^{\infty} g(\boldsymbol{r} + t\boldsymbol{\tau})\ dt\ d\Omega && (10.65)
\end{aligned}
$$

This can be recognized to be a convolution, thus a 3D Fourier transform can be applied on both sides.

$$
\begin{aligned}
\tilde{G}(\boldsymbol{\nu}) &= \int_{\Omega}\int_{t=-\infty}^{\infty}\int_{\boldsymbol{r}=-\infty}^{\infty} g(\boldsymbol{r}+t\boldsymbol{\tau})\ e^{-j2\pi\boldsymbol{\nu}\cdot\boldsymbol{r}}\ d\boldsymbol{r}\ dt\ d\Omega && (10.66)\\
&= \int_{\Omega}\int_{t=-\infty}^{\infty}\int_{\tilde{\boldsymbol{r}}=-\infty}^{\infty} g(\tilde{\boldsymbol{r}})\ e^{-j2\pi\boldsymbol{\nu}\cdot(\tilde{\boldsymbol{r}}-t\boldsymbol{\tau})}\ d\tilde{\boldsymbol{r}}\ dt\ d\Omega && (10.67)\\
&= \int_{\Omega}\int_{t=-\infty}^{\infty} G(\boldsymbol{\nu})\ e^{j2\pi t\boldsymbol{\nu}\cdot\boldsymbol{\tau}}\ dt\ d\Omega && (10.68)\\
&= G(\boldsymbol{\nu})\ \int_{\Omega}\delta(\boldsymbol{\nu}\cdot\boldsymbol{\tau})\ d\Omega \equiv \frac{G(\boldsymbol{\nu})}{H_a(\boldsymbol{\nu})} && (10.69)
\end{aligned}
$$

This implies that backprojected function can be "inverse"-filtered with $H_a(\boldsymbol{\nu})$ to get the correct function.

$$H_a(\boldsymbol{\nu}) = \frac{1}{\int_\Omega \delta(\boldsymbol{\nu}\cdot\boldsymbol{\tau})\ d\Omega} \tag{10.70}$$

Defining κ to be the angle between $\boldsymbol{\tau}$ and $\boldsymbol{\nu}$ and assuming a full coverage ($\Omega = \Omega_{\pi/2}$) gives

$$\frac{1}{H_a(\boldsymbol{\nu})} = \int_{\Omega_{\pi/2}} \delta(|\boldsymbol{\nu}||\boldsymbol{\tau}|\cos\kappa)\ d\Omega = \frac{1}{|\boldsymbol{\nu}|}\int_{\Omega_{\pi/2}} \delta(\cos\kappa)\ d\Omega = \frac{1}{|\boldsymbol{\nu}|}\int_{\phi=-\pi/2}^{\pi/2}\int_{\theta=0}^{\pi} \delta\left(\frac{\cos\kappa}{\cos\phi}\right)\ d\theta\ d\phi \tag{10.71}$$

It is also fairly easy to realize that the integral is independent of the angles of the frequency vector, thus can be derived at, e.g., $\boldsymbol{\mu} = (\mu, 0, 0)$.

$$\begin{aligned}
\frac{1}{H_a(\boldsymbol{\nu})} &= \frac{1}{|\boldsymbol{\nu}|}\int_{\phi=-\pi/2}^{\pi/2}\int_{\theta=0}^{\pi} \delta(\cos\theta\cos\phi)\cos\phi\ d\theta\ d\phi && (10.72)\\
&= \frac{1}{|\boldsymbol{\nu}|}\int_{\phi=-\pi/2}^{\pi/2}\int_{\theta=0}^{\pi} \delta(\cos\theta)\ d\theta\ d\phi && (10.73)\\
&= \frac{\pi}{|\boldsymbol{\nu}|}\int_{\theta=0}^{\pi} \delta(\cos\theta)\ d\theta && (10.74)\\
&= \frac{\pi}{|\boldsymbol{\nu}|} && (10.75)
\end{aligned}$$

Note that the filter is very similar to the one used in the two dimensional version of Filtering After Backprojection. Several authors have derived filters. In the geometry $\Omega_{\pi/2}$ Colsher [4] has derived a valid filter. META more here

10.8 3D line Filtered Backprojection

Analogous to the two dimensional filtered backprojection algorithm the filtering can be done before the backprojection, hence the filtered backprojection algorithm becomes

$$\begin{aligned}
g^\dagger(\theta,\phi,u,v) &= H_b(\theta,\phi,u,v) ** \check{g}(\theta,\phi,u,v) && (10.76)\\
&= \int_{u'=-\infty}^{\infty}\int_{v'=-\infty}^{\infty} h_b(\theta,\phi,u-u',v-v')\ \check{g}(\theta,\phi,u',v')\ du'\ dv' && (10.77)\\
g(\boldsymbol{r}) &= \int_\Omega g^\dagger(\theta,\phi,\boldsymbol{r}\cdot\boldsymbol{\alpha},\boldsymbol{r}\cdot\boldsymbol{\beta})\ d\Omega && (10.78)
\end{aligned}$$

The criterion on the filter in 3D Filtered Backprojection will have to satisfy can be derived from the transformation of a delta-function

$$\begin{aligned}
g(\boldsymbol{r}) &= \delta(\boldsymbol{r}) \ \Rightarrow\ \check{g}(\theta,\phi,u,v) = \delta(u)\delta(v)\ \Rightarrow && (10.79)\\
\delta(\boldsymbol{r}) &= \int_\Omega h_b(\theta,\phi,\boldsymbol{r}\cdot\boldsymbol{\alpha},\boldsymbol{r}\cdot\boldsymbol{\beta})\ d\Omega && (10.80)
\end{aligned}$$

The last equation can also be viewed in the frequency domain

$$\begin{aligned}
1 &= \int_\Omega \left[\int_{-\infty}^{\infty}\int_{-\infty}^{\infty}\int_{-\infty}^{\infty} h_b(\theta,\phi,\boldsymbol{r}\cdot\boldsymbol{\alpha},\boldsymbol{r}\cdot\boldsymbol{\beta})\ e^{-j2\pi\boldsymbol{\nu}\cdot\boldsymbol{r}}\ d\boldsymbol{r}\right]\ d\Omega && (10.81)\\
&= \int_\Omega \left[\int_{-\infty}^{\infty}\int_{-\infty}^{\infty}\int_{-\infty}^{\infty} h_a(\theta,\phi,u,v)\ e^{-j2\pi(t\boldsymbol{\nu}\cdot\boldsymbol{\tau}+u\boldsymbol{\nu}\cdot\boldsymbol{\alpha}+v\boldsymbol{\nu}\cdot\boldsymbol{\beta})}\ d\boldsymbol{p}\right]\ d\Omega && (10.82)\\
&= \int_\Omega H_b(\theta,\phi,\boldsymbol{\nu}\cdot\boldsymbol{\alpha},\boldsymbol{\nu}\cdot\boldsymbol{\beta})\ \delta(\boldsymbol{\nu}\cdot\boldsymbol{\tau})\ d\Omega && (10.83)
\end{aligned}$$

In a given geometry several filters are valid, see [3]. In the geometry $\Omega_{\pi/2}$ a such valid filter is

$$H_b(\theta,\phi,\nu_u,\nu_v) = \frac{1}{\pi}\sqrt{\nu_u^2+\nu_v^2} \tag{10.84}$$

This can be validated by inserting Equation 10.84 in 10.83.

$$\begin{aligned}
& \int_{\Omega_{\pi/2}} H_b(\theta,\phi,\boldsymbol{\nu}\cdot\boldsymbol{\alpha},\boldsymbol{\nu}\cdot\boldsymbol{\beta})\ \delta(\boldsymbol{\nu}\cdot\boldsymbol{\tau})\ d\Omega & (10.85)\\
= & \frac{1}{\pi}\int_{\Omega_{\pi/2}} \sqrt{(\boldsymbol{\nu}\cdot\boldsymbol{\alpha})^2+(\boldsymbol{\nu}\cdot\boldsymbol{\beta})^2}\ \delta(\boldsymbol{\nu}\cdot\boldsymbol{\tau})\ d\Omega & (10.86)\\
= & \frac{1}{\pi}\int_{\Omega_{\pi/2}} \sqrt{(\boldsymbol{\nu}\cdot\boldsymbol{\alpha})^2+(\boldsymbol{\nu}\cdot\boldsymbol{\beta})^2+(\boldsymbol{\nu}\cdot\boldsymbol{\tau})^2}\ \delta(\boldsymbol{\nu}\cdot\boldsymbol{\tau})\ d\Omega & (10.87)\\
= & \frac{1}{\pi}\int_{\Omega_{\pi/2}} |\boldsymbol{\nu}|\ \delta(\boldsymbol{\nu}\cdot\boldsymbol{\tau})\ d\Omega & (10.88)\\
= & \frac{1}{\pi}\int_{\theta=0}^{\pi}\int_{\phi=-\pi/2}^{\pi/2} \delta(\cos\kappa)\cos\theta\ d\phi\ d\theta & (10.89)\\
= & \frac{1}{\pi}\int_{\theta=0}^{\pi}\int_{\phi=-\pi/2}^{\pi/2} \delta(\cos\kappa)\cos\theta\ d\phi\ d\theta = 1 & (10.90)
\end{aligned}$$

In the last line uses the result from Equation 10.71 used and κ is still the angle between $\boldsymbol{\nu}$ and $\boldsymbol{\tau}$.

10.9 Connection between the 3D plane integrals and 3D line integrals

In this section the connection between the 3D line integrals and the 3D plane integrals is established. This can be used to exploit the inverse 3D plane Radon transform, e.g. Filtered Backprojection shown in Equation 10.19 and 10.17 to reconstruct a volume from 3D line integrals.

Assume a plane with parameters ρ_p, θ_p, ϕ_p (index p for plane). From θ_p and ϕ_p an orthonormal basis can be found

$$\boldsymbol{\xi} = \begin{pmatrix} \sin\theta_p\cos\phi_p \\ \sin\theta_p\sin\phi_p \\ \cos\theta_p \end{pmatrix} \quad \boldsymbol{\zeta} = \begin{pmatrix} -\sin\phi_p \\ \cos\phi_p \\ 0 \end{pmatrix} \quad \boldsymbol{\eta} = \begin{pmatrix} \cos\theta_p\cos\phi_p \\ \cos\theta_p\sin\phi_p \\ -\sin\theta_p \end{pmatrix} \tag{10.91}$$

Now all lines in the plane (normal to $\boldsymbol{\xi}$) is to be found. The direction vector $\boldsymbol{\tau}$ of the lines can in general be written as

$$\boldsymbol{\tau} = \boldsymbol{\eta}\cos\omega + \boldsymbol{\zeta}\sin\omega \tag{10.92}$$

The vectors are illustrated in Figure 10.1.

Another useful vector is $\boldsymbol{\chi}$, defined as the vector product between $\boldsymbol{\tau}$ and $\boldsymbol{\xi}$. Using that $\boldsymbol{\xi}$, $\boldsymbol{\eta}$ and $\boldsymbol{\zeta}$ are orthonormal vectors imply that

$$\boldsymbol{\chi} = \boldsymbol{\eta}\sin\omega - \boldsymbol{\zeta}\cos\omega \tag{10.93}$$

Using the basis vectors shown in Figure 10.1 the plane integral $\breve{g}(\rho,\boldsymbol{\xi})$ can be expressed as

$$\begin{aligned}
\breve{g}_\omega(\rho,\boldsymbol{\xi}) &= \int_{r=-\infty}^{\infty}\int_{t=-\infty}^{\infty} g(\rho\boldsymbol{\xi}+r\boldsymbol{\chi}+t\boldsymbol{\tau})\ dt\ dr & (10.94)\\
&= \int_{r=-\infty}^{\infty} \breve{g}(\theta_l,\phi_l,u,v)\ dr & (10.95)
\end{aligned}$$

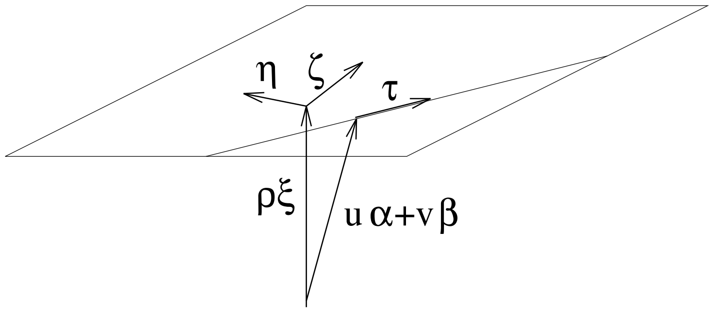

Figure 10.1: The plane with normal vector $\boldsymbol{\xi}$. The line $\boldsymbol{r} = t\boldsymbol{\tau} + u\boldsymbol{\alpha} + v\boldsymbol{\beta}$ lies in the plane.

where θ_l and ϕ_l (The index l stands for line) are the angles corresponding to $\boldsymbol{\tau}$ found from Equation 10.21. The parameters u and v are found from

$$\rho\boldsymbol{\xi} + r\boldsymbol{\chi} = u\boldsymbol{\alpha} + v\boldsymbol{\beta} \tag{10.96}$$

where $\boldsymbol{\alpha}$ and $\boldsymbol{\beta}$ are found from the angles θ_l and ϕ_l.

The result in Equation 10.95 depends on the angle ω. The final estimate of the plane integral may be set to a weighted integral

$$\breve{g}(\rho, \boldsymbol{\xi}) = \frac{1}{\pi}\int_{\omega=0}^{\pi} q(\omega)\ \breve{g}_\omega(\rho, \boldsymbol{\xi})\ d\omega \tag{10.97}$$

$$= \frac{1}{\pi}\int_{\omega=0}^{\pi} q(\omega)\ \int_{r=-\infty}^{\infty} \breve{g}(\theta_l, \phi_l, \boldsymbol{\alpha}\cdot(\rho\boldsymbol{\xi} + r\boldsymbol{\chi}), \boldsymbol{\beta}\cdot(\rho\boldsymbol{\xi} + r\boldsymbol{\chi}))\ dr\ d\omega \tag{10.98}$$

where $q(\omega)$ is a weight designed after the available data. In general it must fulfill

$$\int_{\omega=0}^{\pi} q(\omega)\ d\omega = \pi \tag{10.99}$$

Appendix A

The δ-Function

P.A.M. Dirac introduced a new function in his book on Quantum Mechanics [6], named the δ-function. The function can be defined as

$$\delta(x) = 0 \; \forall \, x \neq 0 \quad \text{and} \quad \int_{-\infty}^{\infty} f(x)\delta(x) \; dx = f(0) \tag{A.1}$$

The function is a part of a new class of functions, the generalized functions. The δ-function is widely used within the theory of Radon transformation, due to the following property.

$$\int_{-\infty}^{\infty} f(x)\delta(x - x_0) \; dx = f(x_0) \tag{A.2}$$

This follows from the definition. Another property is that

$$\delta(ax) = \frac{\delta(x)}{|a|} \tag{A.3}$$

This is a special case of the general property [13].

$$\delta(f(x)) = \sum_{i=1}^{I} \frac{\delta(x - x_i)}{|f'(x_i)|} \tag{A.4}$$

where the set x_i is the zeros of the function $f(x)$. This implies that

$$\int_{-\infty}^{\infty} g(x)\delta(f(x)) \; dx = \sum_{i=1}^{I} \frac{g(x_i)}{|f'(x_i)|} \tag{A.5}$$

Normally the δ-function is easy to use, but in some cases it is very difficult. In these cases the following function is useful.

$$d(x) = \frac{e^{-x^2/\alpha^2}}{\sqrt{\pi}\alpha} \tag{A.6}$$

$$\lim_{\alpha \to 0} d(x) = \delta(x) \tag{A.7}$$

For further information see [6, 8].

Appendix B

Basic Properties of the Radon Transformation

In this appendix several basic properties of the Radon transform are shown. They are based on the properties of the δ-function shown in appendix A.

B.1 Linearity

The first property is that the Radon transform is a linear transform. If α_q is an array of constants, then

$$g(x,y) = \sum_q \alpha_q \; g_q(x,y) \Rightarrow \breve{g}(\rho,\theta) = \sum_q \alpha_q \; \breve{g}_q(\rho,\theta) \tag{B.1}$$

B.2 Shifting

Assume

$$\begin{aligned}
h(x,y) &= g(x-x_0, y-y_0) \;\; \Rightarrow & \text{(B.2)}\\
\breve{h}(\rho,\theta) &= \int_{-\infty}^{\infty}\int_{-\infty}^{\infty} g(x-x_0,y-y_0)\; \delta(\rho - x\cos\theta - y\sin\theta)\; dx\; dy & \text{(B.3)}\\
&= \int_{-\infty}^{\infty}\int_{-\infty}^{\infty} g(\tilde{x},\tilde{y})\; \delta((\rho - x_0\cos\theta - y_0\sin\theta) - \tilde{x}\cos\theta - \tilde{y}\sin\theta)\; d\tilde{x}\; d\tilde{y} & \text{(B.4)}\\
&= \breve{g}(\rho - x_0\cos\theta - y_0\sin\theta, \theta) & \text{(B.5)}
\end{aligned}$$

Note that only the ρ-coordinate is changed.

B.3 Rotation

Here $g(x,y)$ is expressed in polar form, i.e., $g(x,y) = g(r,\phi)$. In this case rotation is fairly easy

$$\begin{aligned}
h(r,\phi) &= g(r,\phi-\phi_0) & \text{(B.6)}\\
\breve{h}(\rho,\theta) &= \int_{-\infty}^{\infty}\int_{0}^{\pi} g(r,\phi-\phi_0)\; \delta(\rho - r\cos\phi\cos\theta - r\sin\phi\sin\theta)\; |r|\; d\phi\; dr & \text{(B.7)}\\
&= \int_{-\infty}^{\infty}\int_{0}^{\pi} \breve{g}(r,\tilde{\phi})\; \delta(\rho - r\cos(\theta-\phi-\phi_0))\; |r|\; d\phi\; dr & \text{(B.8)}\\
&= \breve{g}(\rho,\theta-\phi_0) & \text{(B.9)}
\end{aligned}$$

This is quite obvious. If the coordinate system (x, y) is turned ϕ_0, then the Radon transform is also turned ϕ_0.

B.4 Scaling

Assume a scaling in both coordinates

$$h(x,y) = g\left(\frac{x}{a}, \frac{y}{b}\right), \ a > 0 \text{ and } b > 0 \tag{B.10}$$

In this case the Radon transform can be rewritten

$$\begin{aligned}
\check{h}(\rho,\theta) &= \int_{-\infty}^{\infty}\int_{-\infty}^{\infty} h(x,y)\ \delta(\rho - x\cos\theta - y\sin\theta)\ dx\ dy && \text{(B.11)}\\
&= ab\int_{-\infty}^{\infty}\int_{-\infty}^{\infty} g(\tilde{x},\tilde{y})\ \delta(\rho - a\tilde{x}\cos\theta - b\tilde{y}\sin\theta)\ d\tilde{x}\ d\tilde{y} && \text{(B.12)}\\
&= \frac{ab}{|\gamma|}\int_{-\infty}^{\infty}\int_{-\infty}^{\infty} g(\tilde{x},\tilde{y})\ \delta\left(\frac{\rho}{\gamma} - \tilde{x}\frac{a\cos\theta}{\gamma} - \tilde{y}\frac{b\sin\theta}{\gamma}\right)\ d\tilde{x}\ d\tilde{y} && \text{(B.13)}\\
&\equiv \frac{ab}{|\gamma|}\int_{-\infty}^{\infty}\int_{-\infty}^{\infty} g(\tilde{x},\tilde{y})\ \delta(\tilde{\rho} - \tilde{x}\cos\tilde{\theta} - \tilde{y}\sin\tilde{\theta})\ d\tilde{x}\ d\tilde{y} && \text{(B.14)}\\
&= \frac{ab}{|\gamma|}\ \check{g}(\tilde{\rho},\tilde{\theta}) && \text{(B.15)}
\end{aligned}$$

Now $\tilde{\rho}$ and $\tilde{\theta}$ must be found as functions of ρ and θ. From the equations above it is found that

$$\begin{aligned}
\cos\tilde{\theta} &= \frac{a\cos\theta}{\gamma} \text{ and } \sin\tilde{\theta} = \frac{a\sin\theta}{\gamma} && \text{(B.16)}\\
\cos^2\tilde{\theta} + \sin^2\tilde{\theta} &= 1 \ \Rightarrow\ \gamma = \sqrt{(a\cos\theta)^2 + (b\sin\theta)^2}\ \Rightarrow && \text{(B.17)}\\
\tilde{\rho} &= \frac{\rho}{\sqrt{(a\cos\theta)^2 + (b\sin\theta)^2}} && \text{(B.18)}\\
a\tan\tilde{\theta} &= b\tan\theta \ \Rightarrow\ \tilde{\theta} = \arctan\left(\frac{b}{a}\tan\theta\right) && \text{(B.19)}
\end{aligned}$$

To summerize the equations shown above

$$\begin{aligned}
h(x,y) &= g\left(\frac{x}{a}, \frac{y}{b}\right), \ a > 0 \text{ and } b > 0 \ \Rightarrow && \text{(B.20)}\\
\check{h}(\rho,\theta) &= \frac{ab}{\gamma}\ \check{g}\left(\frac{\rho}{\sqrt{(a\cos\theta)^2 + (b\sin\theta)^2}}, \arctan\left(\frac{b}{a}\tan\theta\right)\right) && \text{(B.21)}
\end{aligned}$$

If using $0 \le \theta < \pi$, then the arctan function is

$$\arctan\left(\frac{b}{a}\tan\theta\right) = \begin{cases} \text{Arctan}\left(\frac{b}{a}\tan\theta\right) & \text{if } 0 \le \theta < \frac{\pi}{2} \\ \text{Arctan}\left(\frac{b}{a}\tan\theta\right) + \pi & \text{if } \frac{\pi}{2} \le \theta < \pi \end{cases} \tag{B.22}$$

B.5 Convolution

Assume the function $h(x, y)$ being a 2D convolution of $f(x, y)$ and $g(x, y)$.

$$h(x,y) = f(x,y) **g(x,y) = \int \int f(x_1,y_1)\ g(x-x_1, y-y_1)\ dx_1\ dy_1 \tag{B.23}$$

Then the Radon transform of $h(x, y)$ is given by

$$\begin{aligned}
\check{h}(\rho,\theta) &= \int\int\int\int f(x_1,y_1)\ g(x-x_1,y-y_1)\ \delta(\rho - x\cos\theta - y\sin\theta)\ dx_1\ dy_1\ dx\ dy \\
&= \int\int f(x_1,y_1) \int\int g(x-x_1,y-y_1)\ \delta(\rho - x\cos\theta - y\sin\theta)\ dx\ dy\ dx_1\ dy_1 \\
&= \int\int f(x_1,y_1)\ \check{g}(\rho - x_1\cos\theta - y_1\sin\theta,\theta)\ dx_1\ dy_1 \\
&= \int\int f(x_1,y_1) \int \check{g}(\rho-\rho_1,\theta)\ \delta(\rho_1 - x_1\cos\theta - y_1\sin\theta,\theta)\ d\rho_1\ dx_1\ dy_1 \\
&= \int \check{g}(\rho-\rho_1,\theta) \int\int f(x_1,y_1)\ \check{g}(\rho_1 - x_1\cos\theta - y_1\sin\theta,\theta)\ dx_1\ dy_1\ d\rho_1 \\
&= \int \check{f}(\rho_1,\theta)\ \check{g}(\rho-\rho_1,\theta)\ d\rho_1 & \text{(B.24)} \\
&= \check{f}(\rho,\theta)\ *\ \check{g}(\rho,\theta) & \text{(B.25)}
\end{aligned}$$

In the previously integrals all limits are from minus infinity to infinity. The result is that the Radon transform of a two dimensional convolution is a one dimensional convolution of the Radon transformed functions with respect to ρ. The result is quite obvious from the Central Slice Theorem shown in Equation 4.6. The two dimensional Fourier transformation of a convolution becomes a product. The product is still a product expressed in polar coordinates. The inverse one dimenional Radon transform of the product becomes a convolution in ρ.

Appendix C

The Shepp-Logan Phantom Brain

A 'famous' model of a brain is the Shepp Logan Phantom. This is a model based on ellipses, which can be Radon transformed analytically. The phantom can be used to test the numerical algorithms and evaluate the numerical errors quantitatively. Using the properties shown in appendix B a sum of ellipses can be transformed analytically, if a circle with radius one can be transformed, as shown on Figure C.1. A unit circle is here defined as

$$g_u(x,y) = \begin{cases} 1 \text{ if } x^2+y^2<1 \\ 0 \text{ otherwise} \end{cases} \tag{C.1}$$

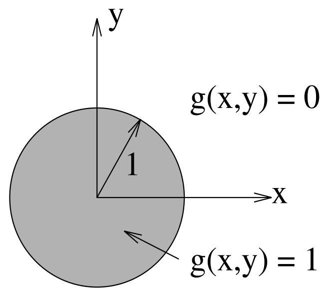

Figure C.1: The unit circle

In this case the function is invariant to rotation around the origin of the coordinate system, thus the Radon transform does not depend on θ. The Radon transform can, e.g., be calculated for $\theta = 0$, as shown on Figure C.2. Due to the constant excitation on the circle, the Radon transform is merely the length of the line crossing the circle.

From Figure C.2 it is found that

$$\breve{g}_u(\rho,\theta) = \begin{cases} 2\sqrt{1-\rho^2} \text{ if } \rho^2<1 \\ 0 \text{ otherwise} \end{cases} \tag{C.2}$$

Using Equation C.2 and the properties shown in Appendix B, it is found that a sum of ellipses can be transformed analytically. If the unit circle is scaled, rotated and shifted an ellipse is formed, shown on Figure C.3.

If the ellipse is called $g_{A,a,b,\phi,x_0,y_0}(x,y)$, then the Radon transform is given by

$$\breve{g}_{A,a,b,\phi,x_0,y_0}(\rho,\theta) = \begin{cases} 2Aab\,\frac{\sqrt{\rho_0^2-(\rho-x_0\cos\theta-y_0\sin\theta)^2}}{\rho_0^2} & \text{if } |\rho-x_0\cos\theta-y_0\sin\theta|<\rho_0 \\ 0 \quad \text{otherwise} \end{cases} \tag{C.3}$$

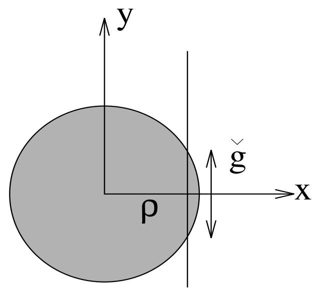

Figure C.2: Radon transformation for $\theta = 0$

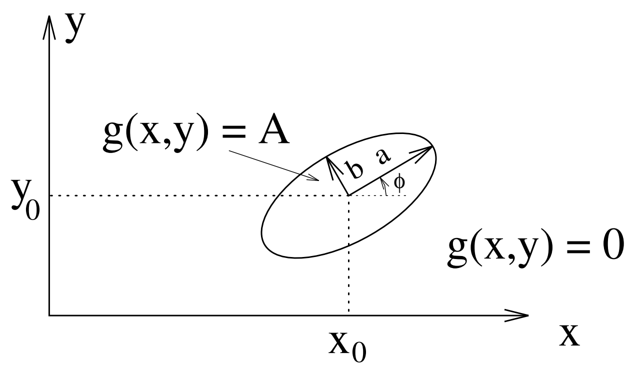

Figure C.3: An ellipse with the relevant parameters indicated

$$\rho_0 \quad = \quad a^2 \cos^2(\theta - \phi) + b^2 \sin^2(\theta - \phi) \tag{C.4}$$

If Q ellipses are given with a set of parameters, then due to the linearity, the Radon transform is a sum

$$g(x, y) \quad = \quad \sum_{q=1}^{Q} g_{A_q, a_q, b_q, \phi_q, x_{0,q}, y_{0,q}}(x, y) \;\Rightarrow \tag{C.5}$$

$$\breve{g}(\rho, \theta) \quad = \quad \sum_{q=1}^{Q} \breve{g}_{A_q, a_q, b_q, \phi_q, x_{0,q}, y_{0,q}}(\rho, \theta) \tag{C.6}$$

The Shepp-Logan Phantom is a sum of ten ellipses with parameters, shown in Table C.1. Note that the ellipse amplitude A does not exactly match those of the original phantom. This choice gives a better contrast.

The resulting phantom brain is shown on Figure C.4 and the corresponding Radon transform is shown on Figure C.5.

A	a	b	x_0	y_0	ϕ
1.0	0.69	0.92	0.0	0.0	0^0
-0.8	0.6624	0.874	0.0	-0.0184	0^0
-0.2	0.11	0.31	0.22	0.0	-18^0
-0.2	0.16	0.41	-0.22	0.0	18^0
0.1	0.21	0.25	0.0	0.35	0^0
0.1	0.046	0.046	0.0	0.1	0^0
0.1	0.046	0.046	0.0	-0.1	0^0
0.1	0.046	0.023	-0.08	-0.605	0^0
0.1	0.023	0.023	0.0	-0.606	0^0
0.1	0.023	0.046	0.06	-0.605	0^0

Table C.1: Parameter settings for the Shepp Logan Phantom.

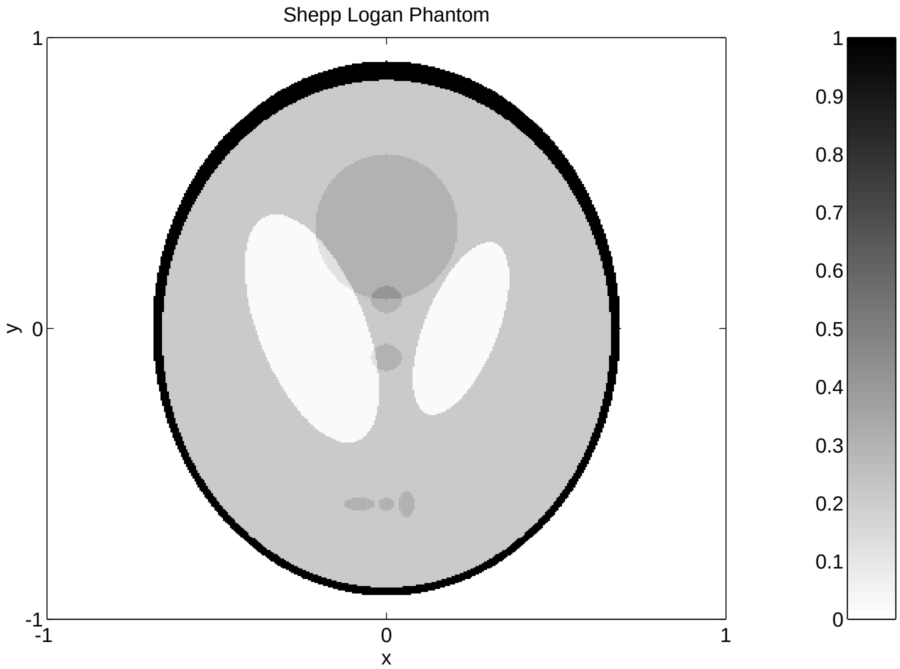

Figure C.4: The Phantom brain

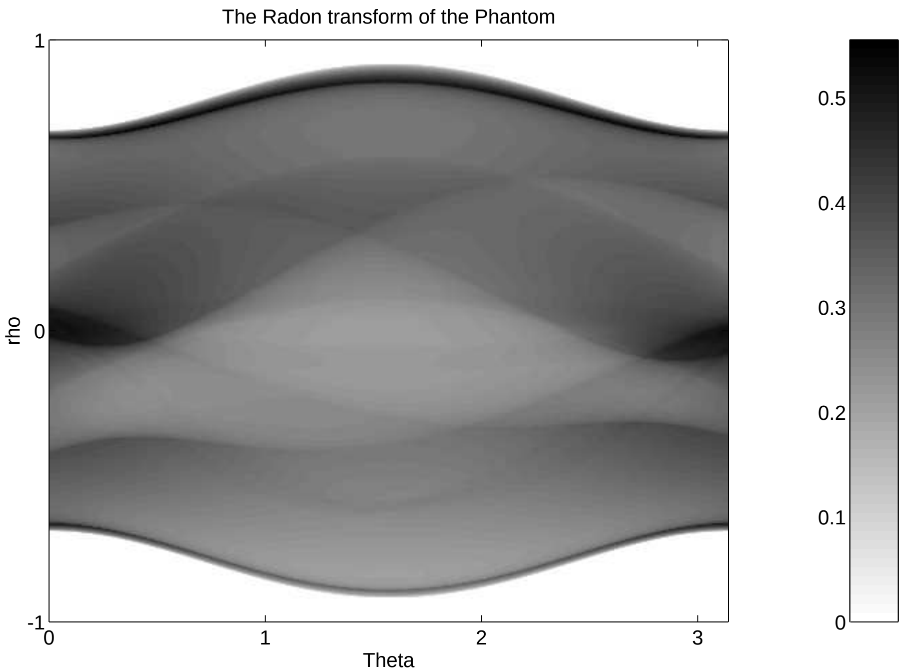

Figure C.5: The corresponding Radon transform

Appendix D

Properties of the 3D line Radon Transform

From the 3D line Radon transform again shown in Equation D.1 several properties are derived.

$$\check{g}(\theta, \phi, u, v) = \int_{-\infty}^{\infty} g(t\boldsymbol{\tau} + u\boldsymbol{\alpha} + v\boldsymbol{\beta})\ dt \tag{D.1}$$

D.1 Linearity

The first crusial property is linearity of the transform.

$$g(\boldsymbol{r}) = \sum_i \kappa_i\ g_i(\boldsymbol{r}) \Rightarrow \tag{D.2}$$

$$\check{g}(\theta, \phi, u, v) = \sum_i \kappa_i\ \check{g}_i(\theta, \phi, u, v) \tag{D.3}$$

where κ_i are a set of arbitrary constants.

D.2 Translation

It is assumed that

$$h(\boldsymbol{r}) = g(\boldsymbol{r} - \boldsymbol{r_0}) \Rightarrow \tag{D.4}$$

$$\check{h}(\theta, \phi, u, v) = \int_{-\infty}^{\infty} g(t\boldsymbol{\tau} + u\boldsymbol{\alpha} + v\boldsymbol{\beta} - \boldsymbol{r_0})\ dt \tag{D.5}$$

Here the translation $\boldsymbol{r_0}$ are resolved after the basis vectors, i.e.,

$$\boldsymbol{r_0} = t_0\boldsymbol{\tau} + u_0\boldsymbol{\alpha} + v_0\boldsymbol{\beta} \tag{D.6}$$

This can be done in an unambiguous way

$$t_0 = \boldsymbol{r_0}\cdot\boldsymbol{\tau} \quad u_0 = \boldsymbol{r_0}\cdot\boldsymbol{\alpha} \quad v_0 = \boldsymbol{r_0}\cdot\boldsymbol{\beta} \tag{D.7}$$

This is inserted in Equation D.5.

$$\check{h}(\theta, \phi, u, v) = \int_{-\infty}^{\infty} g((t - t_0)\boldsymbol{\tau} + (u - u_0)\boldsymbol{\alpha} + (v - v_0)\boldsymbol{\beta})\ dt \tag{D.8}$$

$$= \int_{-\infty}^{\infty} g(t'\boldsymbol{\tau} + (u - u_0)\boldsymbol{\alpha} + (v - v_0)\boldsymbol{\beta})\ dt' \Rightarrow \tag{D.9}$$

$$\check{h}(\theta, \phi, u, v) = \check{g}(\theta, \phi, u - \boldsymbol{r_0}\cdot\boldsymbol{\alpha}, v - \boldsymbol{r_0}\cdot\boldsymbol{\beta}) \tag{D.10}$$

Note that the angular parameters θ and ϕ are not changed.

D.3 Rotation and Scaling

Rotation and and scaling can be controlled by means of a general transformation matrix $\boldsymbol{A}$

$$h(\boldsymbol{r}) = g(\boldsymbol{A}\boldsymbol{r}) \tag{D.11}$$

The diagonal elements of the 3×3 matrix control the individual scaling and the off-diagonal elements are controlling the rotation. The corresponding Radon transform is given by

$$\begin{aligned} \check{h}(\theta,\phi,u,v) &= \int_{-\infty}^{\infty} g(\boldsymbol{A}(t\boldsymbol{\tau} + u\boldsymbol{\alpha} + v\boldsymbol{\beta})\ dt & \text{(D.12)} \\ &= \int_{-\infty}^{\infty} g(t\boldsymbol{A}\boldsymbol{\tau} + u\boldsymbol{A}\boldsymbol{\alpha} + v\boldsymbol{A}\boldsymbol{\beta})\ dt & \text{(D.13)} \end{aligned}$$

This will in general alter the directional vector $\boldsymbol{\tau}$ of the line, i.e., a new direction vector is needed

$$\boldsymbol{A}\boldsymbol{\tau} = \gamma\tilde{\boldsymbol{\tau}} \quad |\tilde{\boldsymbol{\tau}}| = 1 \quad \gamma \geq 0 \tag{D.14}$$

The vector $\tilde{\boldsymbol{\tau}}$ defines cf. Equation 10.21 two corresponding angles $\tilde{\theta}$ and $\tilde{\phi}$, which again defines the two remaining vectors $\tilde{\boldsymbol{\alpha}}$ and $\tilde{\boldsymbol{\beta}}$, cf. Equation 10.23. Now Equation D.14 is inserted into Equation D.13.

$$\check{h}(\theta,\phi,u,v) = \frac{1}{\gamma}\int_{-\infty}^{\infty} g\left(t\tilde{\boldsymbol{\tau}} + \boldsymbol{A}\left(u\boldsymbol{\alpha} + v\boldsymbol{\beta}\right)\right)\ dt \tag{D.15}$$

The next step is to resolve the line offset parameters after the three new tilde vectors, which again can be done unambiguously.

$$\boldsymbol{A}\left(u\boldsymbol{\alpha} + v\boldsymbol{\beta}\right) = t_0\tilde{\boldsymbol{\tau}} + u_0\tilde{\boldsymbol{\alpha}} + v_0\tilde{\boldsymbol{\beta}} \tag{D.16}$$

This implies that the 3D line Radon transform is given by

$$\begin{aligned} \check{h}(\theta,\phi,u,v) &= \frac{1}{\gamma}\int_{-\infty}^{\infty} g\left((t-t_0)\tilde{\boldsymbol{\tau}} + u_0\tilde{\boldsymbol{\alpha}} + v_0\tilde{\boldsymbol{\beta}}\right)\ dt & \text{(D.17)} \\ &= \frac{1}{\gamma}\int_{-\infty}^{\infty} g\left(t'\tilde{\boldsymbol{\tau}} + u_0\tilde{\boldsymbol{\alpha}} + v_0\tilde{\boldsymbol{\beta}}\right)\ dt' & \text{(D.18)} \\ &= \frac{1}{\gamma}\check{g}(\tilde{\theta},\tilde{\phi},u_0,v_0) & \text{(D.19)} \end{aligned}$$

where the four tilde parameters are given by

$$\begin{aligned} \tilde{\boldsymbol{\tau}} &= \begin{pmatrix} \cos\tilde{\phi}\cos\tilde{\theta} \\ \cos\tilde{\phi}\sin\tilde{\theta} \\ \sin\tilde{\phi} \end{pmatrix} = \frac{1}{|\boldsymbol{A}\boldsymbol{\tau}|}\boldsymbol{A}\boldsymbol{\tau}, \quad \tilde{\boldsymbol{\alpha}} = \begin{pmatrix} -\sin\tilde{\theta} \\ \cos\tilde{\theta} \\ 0 \end{pmatrix} \text{ and } \tilde{\boldsymbol{\beta}} = \begin{pmatrix} -\sin\tilde{\phi}\cos\tilde{\theta} \\ -\sin\tilde{\phi}\sin\tilde{\theta} \\ \cos\tilde{\phi} \end{pmatrix} & \text{(D.20)} \\ \gamma &= |\boldsymbol{A}\boldsymbol{\tau}|, \quad u_0 = \tilde{\boldsymbol{\alpha}}\cdot\boldsymbol{A}\cdot(\boldsymbol{\alpha}u + \boldsymbol{\beta}v), \quad v_0 = \tilde{\boldsymbol{\beta}}\cdot\boldsymbol{A}\cdot(\boldsymbol{\alpha}u + \boldsymbol{\beta}v) & \text{(D.21)} \end{aligned}$$

The matrix $\boldsymbol{A}$ can be partitioned in three rotational matrices and one scaling matrix

$$\boldsymbol{A}_x\boldsymbol{A}_x\boldsymbol{A}_x\boldsymbol{S} \tag{D.22}$$

where $\boldsymbol{A}_x$ rotates in the $y - z$ coordinates, e.g.

$$\boldsymbol{A}_x = \begin{pmatrix} 1 & 0 & 0 \\ 0 & \cos\psi_x & \sin\psi_x \\ 0 & -\sin\psi_x & \cos\psi_x \end{pmatrix} \tag{D.23}$$

and $\boldsymbol{A}_y$ rotates in the $x-z$ coordinates, e.g.

$$\boldsymbol{A}_y = \begin{pmatrix} \cos\psi_y & 1 & \sin\psi_y \\ 0 & 1 & 0 \\ -\sin\psi_y & 1 & \cos\psi_y \end{pmatrix} \tag{D.24}$$

and finally $\boldsymbol{A}_z$ rotates in the $x-y$ coordinates, e.g.

$$\boldsymbol{A}_z = \begin{pmatrix} \cos\psi_z & \sin\psi_z & 0 \\ -\sin\psi_z & \cos\psi_z & 0 \\ 0 & 0 & 1 \end{pmatrix} \tag{D.25}$$

The scaling matrix $\boldsymbol{S}$ is here chosen to be the last because the scaling interpretation is by far easier when applied directly on the base function $g(\boldsymbol{r})$. The matrix can be chosen to

$$\boldsymbol{S} = \begin{pmatrix} \frac{1}{S_x} & 0 & 0 \\ 0 & \frac{1}{S_y} & 0 \\ 0 & 0 & \frac{1}{S_z} \end{pmatrix} \tag{D.26}$$

The scaling parameters in the diagonal is chosen so they directly relate to length in the new function $h(\boldsymbol{r})$. The total rotation and scaling matrix defined in Equation D.22 multiplied together becomes

$$\boldsymbol{A} = \begin{pmatrix} \frac{\cos\psi_x\cos\psi_y}{S_x} & \frac{\cos\psi_y\sin\psi_x}{S_y} & \frac{\cos\psi_y\sin\psi_x}{S_z} \\ -\frac{\cos\psi_z\sin\psi_x+\cos\psi_x\sin\psi_y}{S_x} & \frac{\cos\psi_x\cos\psi_z-\sin\psi_x\sin\psi_y\sin\psi_z}{S_y} & \frac{\cos\psi_y\sin\psi_z}{S_z} \\ \frac{\sin\psi_x\sin\psi_z-\cos\psi_x\cos\psi_z\sin\psi_y}{S_x} & -\frac{\cos\psi_z\sin\psi_x\sin\psi_y+\cos\psi_x\sin\psi_z}{S_y} & \frac{\cos\psi_y\cos\psi_z}{S_z} \end{pmatrix} \tag{D.27}$$

D.4 Analytical Radon Transformation

Along with the basic rules of the 3D line Radon transform it is very useful to have a set of base 3D functions and their corresponding Radon transform. In the following the Radon transform of the unit ball and a Gaussian bell are derived. This can be used to produce more complex functions written as a weighted sum of shifted, rotated and scaled primitives.

D.4.1 The ball

The first primitive is the unit ball, i.e.,

$$g_{\text{ball}}(x,y,z) = \begin{cases} 1 & \text{for } x^2+t^2+z^2 < 1 \\ 0 & \text{for } x^2+t^2+z^2 \geq 1 \end{cases} \tag{D.28}$$

Due to the rotational symmetry of the primitive the corresponding Radon transform cannot depend on the two angular parameters θ and ϕ, thus the Radon transform is derived in a rotated coordinate system with $\boldsymbol{\tau}$ lying along the x-axis and the vector $\boldsymbol{r_0} = u\boldsymbol{\alpha} + v\boldsymbol{\beta}$ along the y-axis. As illustrated in Figure D.1 is the Radon transform merely the distance between the two intersection points between the line and the ball.

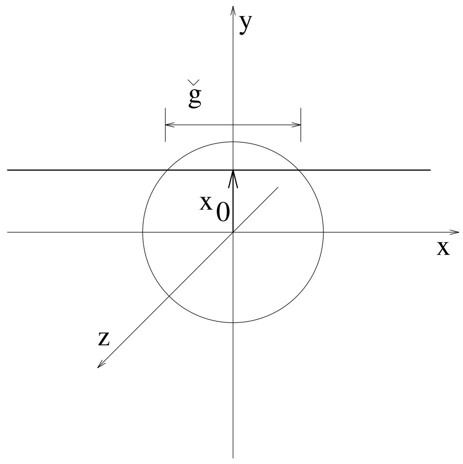

Figure D.1: The unit ball.

The length of $\boldsymbol{r_0}$ is $\sqrt{u^2+v^2}$, which implies that the Radon transform can be calculated as

$$\check{g}_{\text{ball}}(\theta,\phi,u,v) = \int_{-\infty}^{\infty} g_{\text{ball}}\left(t,\sqrt{u^2+v^2},0\right)\,dt \;\Rightarrow \tag{D.29}$$

$$\check{g}_{\text{ball}}(\theta,\phi,u,v) = \begin{cases} 2\sqrt{1-u^2-v^2} & \text{for } u^2+v^2<1 \\ 0 & \text{for } u^2+v^2\geq 1 \end{cases} \tag{D.30}$$

D.4.2 The Gaussian bell

The Gaussian bell is another "easy" primitive.

$$g_{\text{gauss}}(x,y,z) = \exp(-x^2-y^2-z^2) \tag{D.31}$$

Again the function has rotational symmetry, hence the Radon transform does not depend on the angular parameters θ and ϕ, and the Radon transform can, e.g., be derived as

$$\check{g}_{\text{gauss}}(\theta,\phi,u,v) = \int_{-\infty}^{\infty} \exp(-t^2-u^2-v^2)\,dt \;\Rightarrow \tag{D.32}$$

$$\check{g}_{\text{gauss}}(\theta,\phi,u,v) = \sqrt{\pi}\exp(-u^2-v^2) \tag{D.33}$$

Bibliography

[1] Caroline Axelsson. *Direct Fourier Methods in 3D-Reconstruction from Cone-Beam Data.* PhD thesis, Linköbing University, Dep. of Electrical Engineering, S-581 83 Linköbing, Sweden, Jan. 1994. E-mail caroline@isy.liu.se.

[2] Yair Censor. Finite series-expansion reconstruction methods. In *Proc. of the IEEE*, volume 71, pages 409–419, March 1983.

[3] R. Clack. Towards a complete description of three-dimensional filtered backprojection. *Physics in Medicine & Biology*, 37(3):645–660, March 1992.

[4] James G. Colsher. Fully three-dimensional positron emission tomography. *Physics in Medicine and Biology*, 25(1):103–115, 1980.

[5] S. R. Deans. *The Radon Transform and Some of Its Applications.* Krieger Publishing Company, Malabar, Florida, 1993. Previously John Wiley & Sons Inc., 1983.

[6] P. A. M. Dirac. *The Principles of Quantum Mechanics.* Oxford Science Publications, Clarendon, 4. edition, 1984.

[7] P. R. Edholm and G. T. Herman. Linograms in image reconstruction from projections. *IEEE trans. MI*, 6(4):301–307, Dec. 1987.

[8] Gel'fand *et al.* *Generalized Functions*, volume 5. Academic Press, 1964.

[9] William H. Press *et. al.* *Numerical Recipes in C.* Cambridge University Press, 2. edition, 1992.

[10] G. H. Golub and C. F. Van Loan. *Matrix Computations.* The Johns Hopkins University Press, Baltimore and London second, 1991.

[11] Per Christian Hansen. Regularization tools; a matlab package for analysis and solution of discrete ill-posed problems. Report UNIC-92-03, UNIC, UNIC, Technical University of Denmark, DK-2800 Lyngby, 1992.

[12] Gabor T. Herman and Lorraine B. Meyer. Algebraric reconstruction techniques can be mad computationally efficient. *IEEE trans. on Medical Imaging*, 12(3):600–609, Sep. 1993.

[13] A. K. Jain. *Fundamentals of Digital Image Processing.* Prentice Hall, 1989.

[14] S. Kaczmarz. Angenährte auslösung von systemen linearer gleichungen. *Bull. Int. Acad. Pol. Sci. Lett. A*, 35:355–357, 1937.

[15] Maria Magnusson. *The Linogram Method for Image Reconstruction from Projections.* PhD thesis, Linköbings tekniska högskola, Dep. of Electrical Engineering, S-581 83 Linköbing, Sweden, 1989. Revised version 1993.

[16] R. M. Mersereau. Recovering multidimensional signals from their projections. *Computer Graphics and Image Processing*, 1:179–195, 1973.

[17] Frank Natterer. *The Mathematics of Computerized Tomography.* John Wiley & Sons, 1986.

[18] S. S. Orlov. Theory of three dimensional reconstruction. 1. conditions for a complete set of projections. *Sov. Phys. Crystallogr.*, 20(3):312–314, 1975.

[19] S. S. Orlov. Theory of three dimensional reconstruction. the recovery operator. *Sov. Phys. Crystallogr.*, 20(4):429–433, 1975.

[20] Athanasios Papoulis. *Probability, Random Variables and Stochastic Processes.* McGraw-Hill, 2. edition, 1984.

[21] Simon Boel Pedersen. *Signalanalyse I-III.* Electronics Institute, Technical University of Denmark, 1992. Lecture notes for DTU course 4231 (In danish).

[22] D. Townsend R. Clack and M. Defrise. An algorithm for three-dimensional reconstruction incorporating cross-plane rays. *IEEE Transactions on Medical Imaging*, MI-8(1):32–42, 1989.

[23] Johann Radon. Über die bestimmung von funktionen durch ihre integralwerte längs gewisser mannigfaltigkeiten. *Ber. Ver. Sächs. Akad. Wiss. Leipzig, Math-Phys. Kl.*, 69:262–277, April 1917. In german. English translation in S. R. Deans: The Radon Transform and Some of Its Applications.

[24] A. Rosenfeld and A. C. Kak. *Digital Picture Processing*, volume 1. Academic Press, 2. edition, 1982.

[25] L. A. Shepp and J. B. Krustal. Computerized tomography: The new medical x-ray technology. *Am. Math. Monthly*, 85:420–439, April 1978.

[26] Peter Toft. Radontransformation. Lecture note for dtu course 4235,, Electronics Institute, Technical University of Denmark, 1994. In Danish.